

Article

Discovery of New Uracil and Thiouracil Derivatives as Potential HDAC Inhibitors

Omnia R. Elbatrawy¹, Mohamed Hagra^{2,*}, Moshira A. El Deeb¹, Fatimah Agili³, Maghawry Hegazy⁴, Ahmed A. El-Husseiny^{4,5}, Mahmoud Mohamed Mokhtar⁴, Samy Y. Elkhawaga⁴, Ibrahim H. Eissa^{6,*} and Samar El-Kalyoubi^{7,*}

- ¹ Pharmaceutical Organic Chemistry Department, Faculty of Pharmacy (Girls), Al-Azhar University, Cairo 11823, Egypt; omniaelbatrawy2@gmail.com (O.R.E.); moshiraadeleldeeb.pharmg@azhar.edu.eg (M.A.E.D.)
- ² Pharmaceutical Organic Chemistry Department, Faculty of Pharmacy (Boys), Al-Azhar University, Cairo 11884, Egypt
- ³ Chemistry Department, Faculty of Science (Female Section), Jazan University, Jazan 82621, Saudi Arabia; fatmah2000@gmail.com
- ⁴ Biochemistry and Molecular Biology Department, Faculty of Pharmacy (Boys), Al-Azhar University, Cairo 11884, Egypt; drmegawry@azhar.edu.eg (M.H.); ahmedabdullah1984@azhar.edu.eg (A.A.E.-H.); mahmoud.mokhtar@azhar.edu.eg (M.M.M.); syussuf2012@azhar.edu.eg (S.Y.E.)
- ⁵ Department of Biochemistry, Faculty of Pharmacy, Egyptian Russian University, Badr City 11829, Cairo, Egypt
- ⁶ Pharmaceutical Medicinal Chemistry & Drug Design Department, Faculty of Pharmacy (Boys), Al-Azhar University, Cairo 11884, Egypt
- ⁷ Department of Pharmaceutical Organic Chemistry, Faculty of Pharmacy, Port Said University, Port Said 42511, Egypt
- * Correspondence: m.hagra@azhar.edu.eg (M.H.); ibrahimeissa@azhar.edu.eg (I.H.E.); s.elkalyoubi@hotmail.com (S.E.-K.)



Citation: Elbatrawy, O.R.; Hagra, M.; El Deeb, M.A.; Agili, F.; Hegazy, M.; El-Husseiny, A.A.; Mokhtar, M.M.; Elkhawaga, S.Y.; Eissa, I.H.; El-Kalyoubi, S. Discovery of New Uracil and Thiouracil Derivatives as Potential HDAC Inhibitors. *Pharmaceuticals* **2023**, *16*, 966. <https://doi.org/10.3390/ph16070966>

Academic Editor: Francesca Musumeci

Received: 29 May 2023
Revised: 25 June 2023
Accepted: 3 July 2023
Published: 6 July 2023



Copyright: © 2023 by the authors. Licensee MDPI, Basel, Switzerland. This article is an open access article distributed under the terms and conditions of the Creative Commons Attribution (CC BY) license (<https://creativecommons.org/licenses/by/4.0/>).

Abstract: Background: Histone deacetylase inhibitors (HDACIs) are a relatively new class of potential drugs for treating cancer. **Aim:** Discovery of new anticancer agents targeting HDAC. **Methods:** New uracil and thiouracil derivatives panels were designed and synthesized as HDAC inhibitors. The synthesized compounds were tested against MCF-7, HepG2, and HCT-116. HDAC1 and HDAC4 inhibitory activities of these compounds were tested. The most active member was tested for its potential against cell cycle, apoptosis, caspase-3, and caspase-8. Docking studies were carried out against HDAC1. **Results:** Compounds **5a**, **5b**, **5f**, **5i**, **5k**, and **5m** exhibited promising cytotoxic activities. HDAC1 and HDAC4 inhibitory activities of these compounds were tested. Regarding the HDAC1 inhibitory activity, compound **5m** was the most potent member ($IC_{50} = 0.05 \mu\text{g/mL}$) compared to trichostatin A ($IC_{50} = 0.0349 \mu\text{g/mL}$). For HDAC4, compound **5m** showed superior activity ($IC_{50} = 2.83 \mu\text{g/mL}$) than trichostatin A ($IC_{50} = 3.349 \mu\text{g/mL}$). Compound **5m** showed a high potential to arrest the HCT116 cell cycle at the G0-G1 phase. In addition, it showed an almost 17 times apoptotic effect (37.59%) compared to the control cells (2.17%). Furthermore, Compound **5m** showed significant increases in the levels of caspase-3 and caspase-8. Finally, the uracil and thiouracil derivatives showed accepted binding mods against HDAC. **Conclusions:** Compound **5m** has potential anticancer activity targeting HDAC with a significant apoptotic effect.

Keywords: anticancer; in silico studies; HDAC inhibitors; thiouracil; uracil

1. Introduction

Cancer continues to be one of humanity's most significant public health issues, despite the enormous efforts to combat it [1]. According to the WHO, cancer was the leading cause of death worldwide in 2020, accounting for almost 10 million deaths, or about one in every six [2]. As a result, cancer is viewed as a serious issue for both the economy of nations and the economies of individuals [3,4]. Examples of how the complication of cancer

pathology manifests itself include oncogenic mutations, multi-drug resistance, and the activation of compensatory mechanisms [5–7]. Finding anticancer options that are more potent and less harmful, based on the various biological and molecular characteristics of cancer pathogenesis, is therefore crucial.

One of the main epigenetic pathways implicated in cancer development is histone acetylation [8]. Histone acetylation is a required precursor to other processes of epigenetic modifications, such as methylation or phosphorylation, and it not only causes genetic alterations on its own [9,10]. Histone acetyltransferases (HAT) and histone deacetylases (HDAC) are two antagonistic categories of enzymes that control the process of histone acetylation. As lysine residues on histone and non-histone proteins are acetylated, heterochromatin is transformed into euchromatin, whereas HDACs play the opposite role by deacetylating chromatin to return it to its more condensed condition [11]

A relatively emerging family of prospective medications for treating hyperproliferative illnesses is histone deacetylase inhibitors (HDACIs) [12–14]. These inhibitors bind directly to the HDAC active site and block substrate access, producing an accumulation of acetylated histone [15–17]. They can affect differentiation, growth arrest, and/or apoptosis in transformed cell cultures due to their diverse biological activities [18,19]. There is a high demand for novel HDACIs as HDACs have become a key tactic in anticancer drug research [20,21]. Some families of tiny, powerful HDACIs have recently been discovered (Figure 1) [22,23].

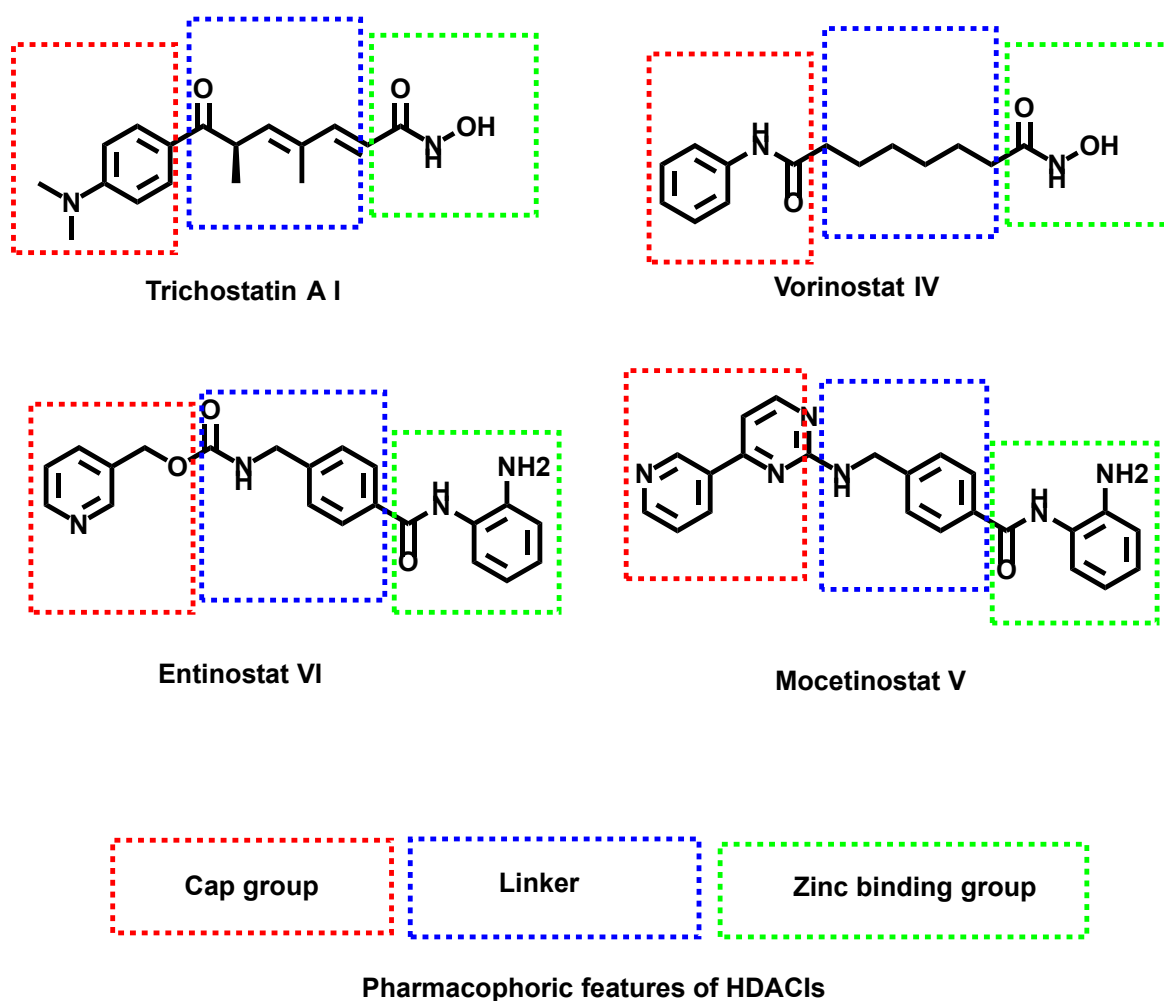


Figure 1. Some reported HDAC inhibitors and their basic pharmacophoric features.

HDACIs should have a cap group, a spacer, and a functional group as basic pharmacophores [24]. The reported functional groups are hydroxamic acids, carboxylic acids, and phenylene diamines [25].

Besides, uracil and thiouracil moieties are important N-containing heterocycles in medicinal chemistry and drug discovery [26] due to their wide scope of biological activity [26], especially antitumor activities [27]. So, our goal is the design and synthesis of new uracil and thiouracil-containing derivatives targeting HDAC with promising effects against cancer.

Rationale of Molecular Design

Studying the SAR of the HDAC inhibitors class revealed three pharmacophoric features essential for maximal fitting in the active site of HDAC. These features include (i) a zinc-binding region group (ZBG) which can interact with the zinc atom in the active site, (ii) a linker moiety that can occupy the tubular access of the active site, and (iii) a cap group which can occupy the surface recognition motif [28] (Figure 2).

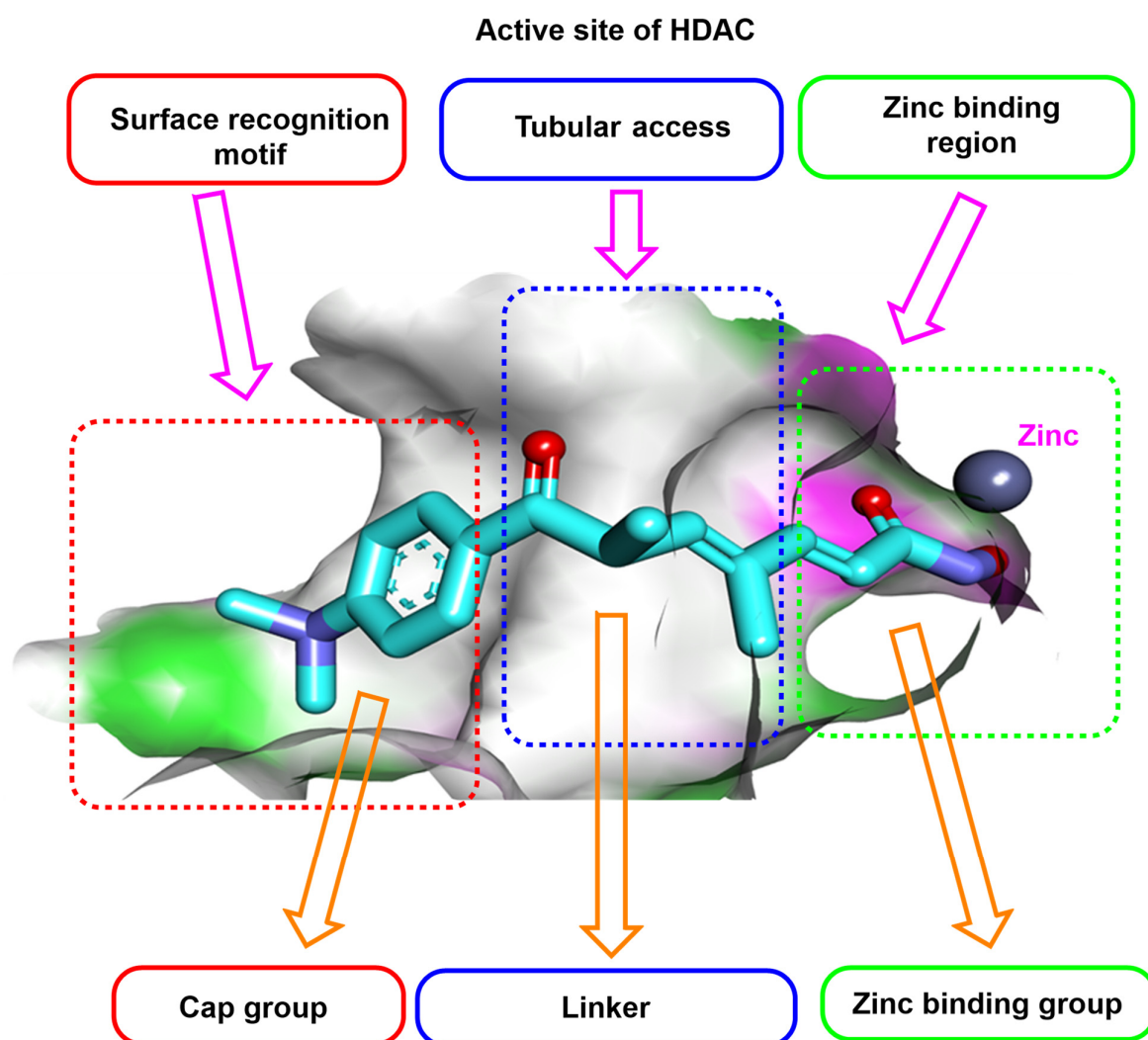


Figure 2. Schematic diagram of trichostatin A occupying the active site of HDAC and the essential pharmacophoric features of HDAC inhibitors.

In this work, we aimed to synthesize new compounds targeting HDAC. The new compounds were designed to possess the pharmacophoric features of HDAC inhibitors. Many derivatives were applied in this work to reach a good insight into the SAR of the synthesized compounds as potential anticancer agents.

The designed compounds varied in their different pharmacophoric features. For the zinc-binding region, two bioisosters were used. These isosters are the substituted thiouracil (5a–g and 6a–d) and uracil (5h–m and 7a–c) derivatives. Different benzyl derivatives (5a–g and 5i–m) were used as linkers. In one compound (5h), a methylene group was used as a linker. Additional series (6a–d and 7a–c) comprise different cyclic structures as a linker moiety. Regarding the cap group, it was thiouracil (5a–g and 6a–d) and uracil (5h–m and 7a–c) derivatives (Figure 3).

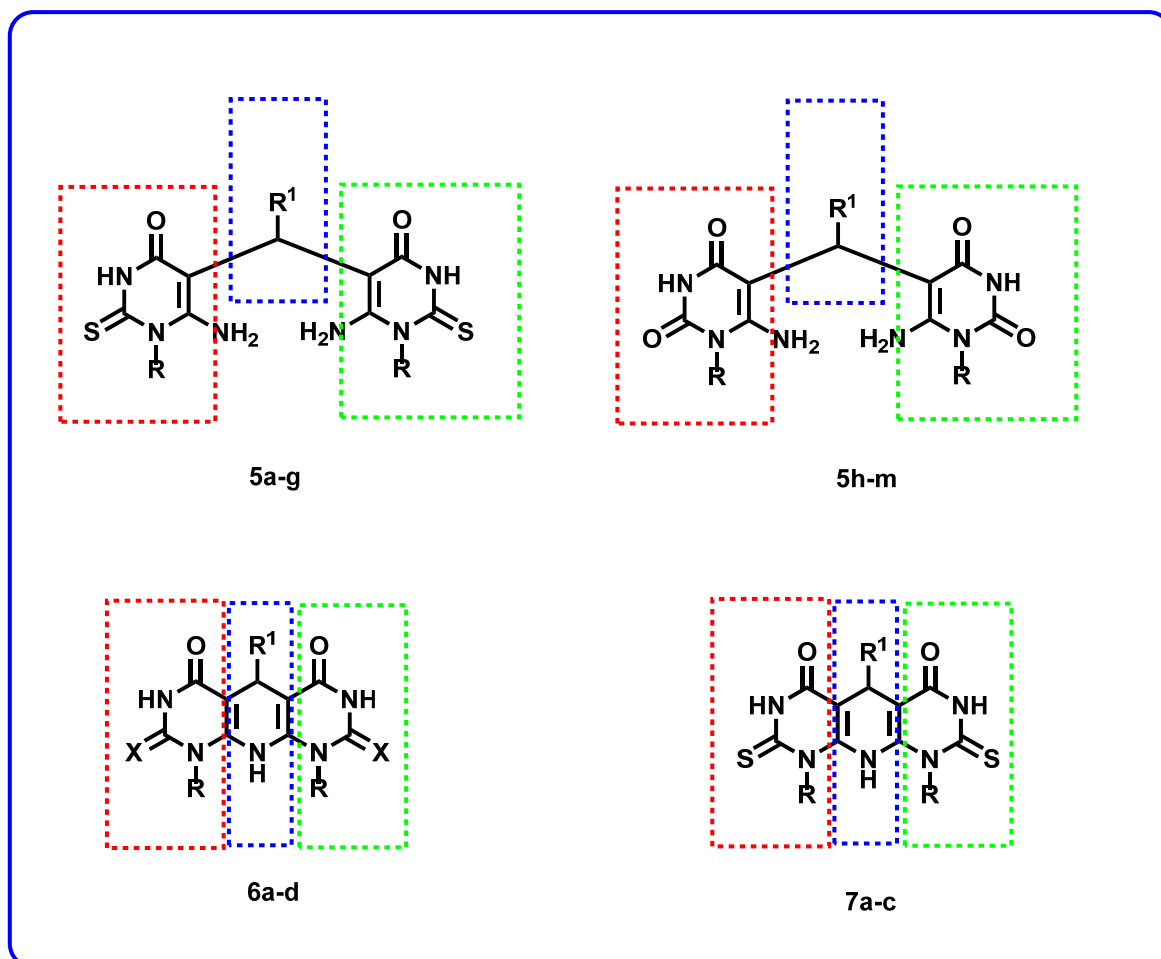
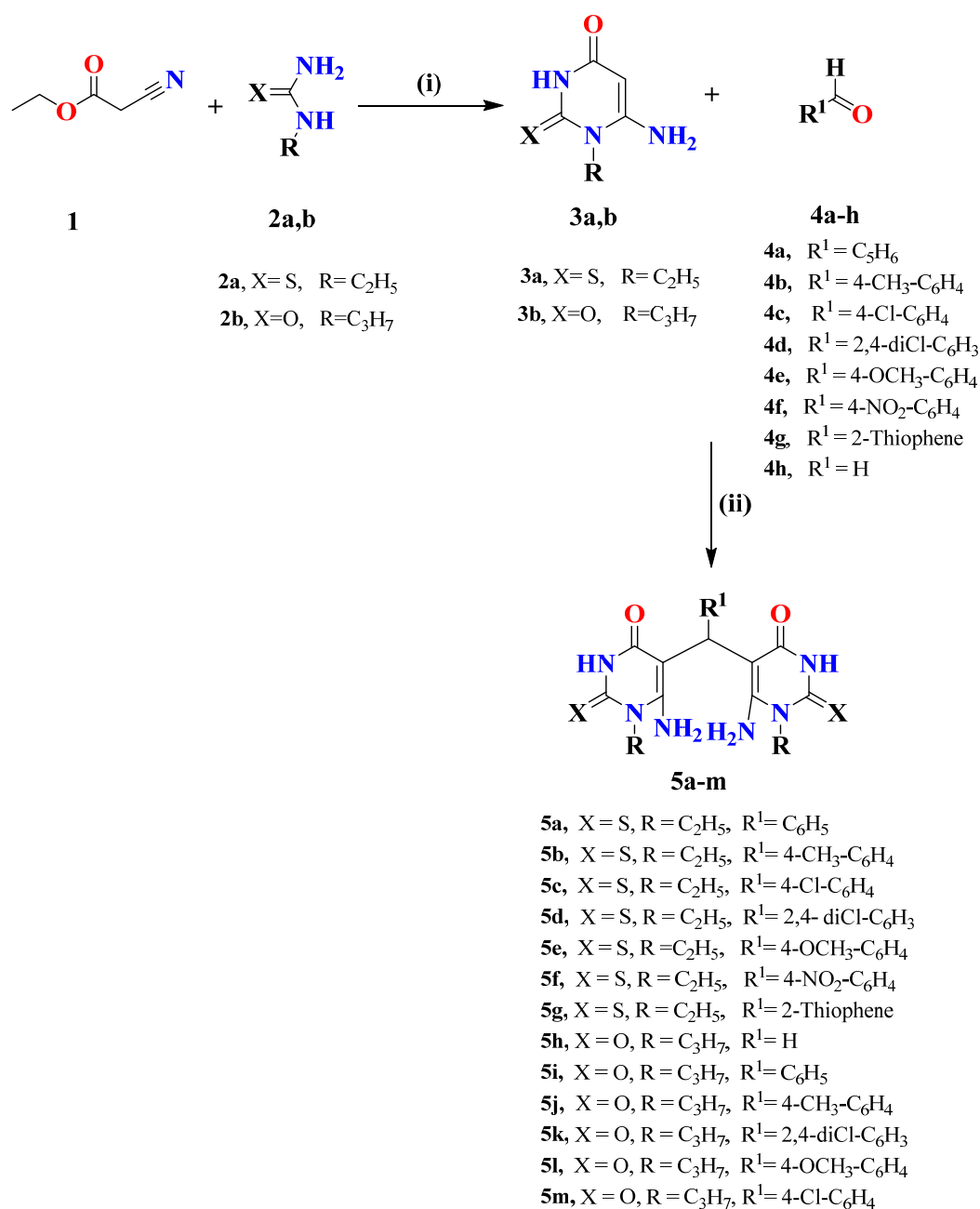


Figure 3. The target compounds represent the essential pharmacophoric features of HDAC inhibitors.

2. Results and Discussion

2.1. Chemistry

The ability of 6-aminouracil to react with aliphatic or aromatic carbonyl compounds [29–35] has been amply demonstrated up till now. The search for new biologically active substances has fueled interest in these reactions, as the presence of a uracil moiety that is a pharmacophore in an organic molecule frequently provides the molecule with some kind of biological effect. Significant progress has been made in uracil derivatives in the field of chemistry. Our protocol is directed towards synthesized novel derivatives of 5,5'-(arylmethylene)bis(6-aminouracils) and dipyrimidopyridines. 6-Amino-2-oxo(thioxo)pyrimidine-4-ones **3a,b** was used as starting material and prepared according to the reported methods [29–34] as shown in Scheme 1.



Scheme 1. Synthesis of compounds **5a–m**. Reagents and conditions: (i) C₂H₅ONa, EtOH, heating under reflux, 8–10 h.; (ii) EtOH, c.HCl, R.T., 2–3 h.

The condensation of appropriate aliphatic or aromatic aldehydes (at the ratio carbonyl compound to aminouracils 1:2) with compounds **3a,b** in ethanol in the presence of HCl at room temperature resulting in 5,5'-bisdiaminopyrimidines **5a–m** in good yields. The latter compounds undergo intermolecular dehydration, as shown in Figure 4. The desired compounds **5a–m** were approved by spectral data ¹H-, ¹³C NMR, IR, and Mass spectra. ¹H NMR spectra of compounds **5a–m** showed a characteristic singlet signals of CH-5 at the range of δ 5.37–6.05 ppm, as well as broad singlet signals characteristic for the 2NH₂-6 group at δ 7.05–7.95 ppm.

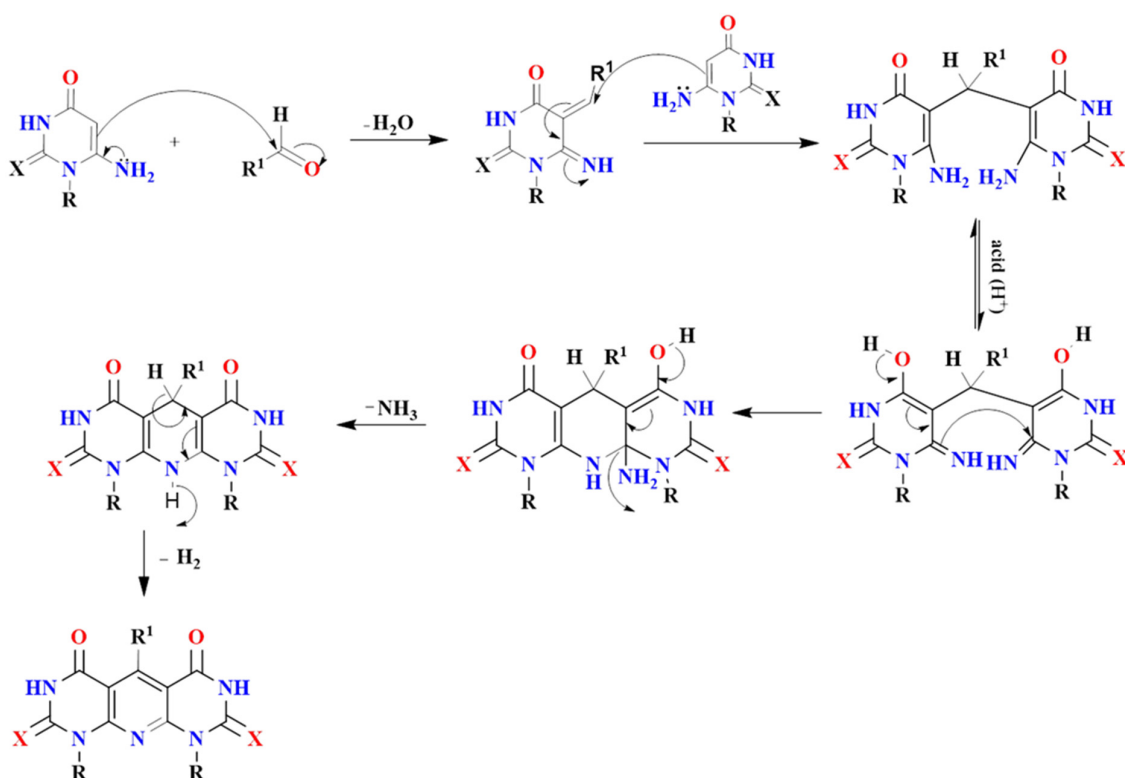


Figure 4. A plausible reaction mechanism for synthesized compounds **5a–m**, **6a–d** and **7a–c**.

Dipyrimidopyridine derivatives **6a–d** were synthesized in good yields from refluxing of compounds **5a**, **f**, **h**, **l** with a mixture of AcOH/c.HCl for 2.5 h (Scheme 2). The reaction proceeds through the same idea of the Hantzsch reaction via intramolecular cyclization accompanied by the evolution of NH₃ due to the attack of the amino group of one unit to the electrophilic carbon center of C=NH, as illustrated in Figure 4. The novel compounds were revealed by ¹H NMR, ¹³C NMR, IR, and Mass spectra. ¹H NMR of compounds **6a–c** exhibit the disappearance of the four singlet signal protons characteristic for 2NH₂ groups and the appearance of a singlet signal of NH-10 at δ 7.77–7.37 ppm and another singlet signal characteristic for CH-5 at δ 5.46–5.75 ppm. Moreover, compound **6d** showed a characteristic singlet signal for NH-10 at δ 7.18 and CH₂-5 at δ 3.49 ppm. A characteristic C-5 signal at the δ 80–90 ppm range was noticed in ¹³C NMR for the mentioned compounds.

On the other hand, Refluxing compounds **5c**, **e**, **g** with a mixture of AcOH/c.HCl for 4–5 h take place through intramolecular oxidative cyclization afforded **7a–c** (Scheme 2), which is proved by all spectral data. ¹H NMR proved, without doubt, the formation of oxidative cyclized compounds **7a–c** via the disappearance of the singlet signal of NH-10 at the region of δ 7 ppm as well as the clearance of the spectra from the singlet signal of CH-5 at the range δ 5.50–5.70 ppm. Moreover, the characteristic C-5 signal appeared at the normal deshielded aromatic region in ¹³C NMR, which proved the complete aromatization of the pyridine ring. A plausible reaction mechanism might be illustrated as follows in Figure 4.

2.2. Biological Testing

2.2.1. In Vitro Cytotoxic Activities

Anti-proliferative effect of the target compounds was assessed against a panel of tumor cell lines, including MCF-7 (human breast cancer cell line), HepG2 (human liver carcinoma cell line), colorectal carcinoma (HCT-116) using MTT assay [36]. Sorafenib was used as a reference drug. From the results presented in Table 1, it is clear that **5a**, **5g**, and **5f** has promising anti-proliferative effect against MCF-7 with IC₅₀ values of 11 ± 1.6, 21 ± 2.2, 9.3 ± 3.4 μM, respectively compared to sorafenib (IC₅₀ = 141 ± 3 μM). In addition, compound **5b** showed high activity against HCT-116 cells with an IC₅₀ value of 21 ± 2.4 μM

Table 1. In vitro cytotoxic activities of the target compounds against MCF-7, HepG2, and HCT-116 cell lines.

Comp.	Cytotoxicity IC ₅₀ (μM) ^a			
	MCF-7	HepG-2	HCT-116	WI-38
5a	11 ± 1.6	39 ± 2.5	88 ± 2.4	-
5b	55 ± 2.8	51 ± 4.0	21 ± 2.4	-
5c	77 ± 2.3	89 ± 2.4	97 ± 1.2	-
5d	62 ± 2.1	40 ± 2.7	281 ± 2.1	-
5e	60 ± 0.49	42 ± 2.0	90 ± 3.0	-
5f	9.3 ± 3.4	49 ± 0.17	71 ± 2.1	-
5g	21 ± 2.2	33 ± 3.8	68 ± 1.8	-
5h	88 ± 2.5	52 ± 3.2	91 ± 1.9	-
5i	261 ± 2.5	4 ± 1.0	64 ± 2.1	-
5j	71 ± 2.0	38 ± 1.8	400 ± 2.4	-
5k	242 ± 2.0	5 ± 2.0	80 ± 2.6	-
5l	381 ± 1.5	31 ± 2.0	83 ± 1.9	-
5m	52 ± 3.5	3.3 ± 0.56	78 ± 2.0	65.67 ± 1.7
6a	333 ± 2.9	220 ± 3.0	291 ± 3.5	-
6b	577 ± 20	184 ± 3.7	299 ± 2.0	-
6c	435 ± 4.3	114 ± 2.2	466 ± 4.6	-
6d	413 ± 1.3	168 ± 1.5	361 ± 2.0	-
7a	472 ± 3.2	189 ± 4.8	361 ± 1.9	-
7b	871 ± 3.2	173 ± 4.5	301 ± 3.4	-
7c	450 ± 2.2	221 ± 2.5	243 ± 2.2	-
Sorafenib	141 ± 3.0	17 ± 2.3.0	177 ± 0.9	-
Staurosporine	-	-	-	51.48 ± 2.2

^a All IC₅₀ values are calculated as the mean of at least three experiments.

Depending on the cytotoxicity against MCF-7, we can reach more details about SAR. For the thiouracil derivatives with open-chain linkers (**5a–g**), it was found that activity decreased upon substitution at the linker region as the order of 4-nitrophenyl > phenyl > thiophene > 4-methylphenyl > 4-methoxyphenyl > 2,4-dichlorophenyl > 4-chlorophenyl.

For the uracil derivatives with open chain linkers (**5h–m**), it was found that activity decreased upon substitution at the linker region as the order of 4-chlorophenyl > 4-methylphenyl > H > 2,4-dichlorophenyl > phenyl > 4-methoxyphenyl.

For the thiouracil derivatives with cyclic linkers (**6a,b**), it was found that the substitution phenyl moiety (**6a**) is more advantageous than the substitution with 4-nitrophenyl moiety (**6b**).

For the uracil derivatives with cyclic linkers (**6c,d**), it was found that the unsubstituted cyclic linker (**6d**) is more advantageous than the substituted one with 4-methoxyphenyl moiety (**6c**).

Compared to the activity of the compound, the thiouracil derivatives **6c** (bearing a propyl moiety at both cap and zinc binding group) and **7b** (bearing an ethyl moiety at both cap and zinc binding group) indicated that the substitution with propyl moiety is better for biological activity.

2.2.3. HDAC1 and HDAC4 Inhibitory Assay

HDAC1 plays a critical role in proliferating and senescent cells in culture and young and old tissues in vivo [37]. HDAC1 levels are also essential for regulating apoptosis [38]. Basic and clinical experimental evidence has established that HDAC4 performs various functions [39]. Accordingly, HDAC1 and HDAC4 were selected for testing in this work.

To assess the mechanism of cytotoxicity of the synthesized compounds, HDAC1 and HDAC4 inhibitory activities of the most cytotoxic compounds (**5a**, **5b**, **5f**, **5i**, **5k**, and **5m**) were tested. Trichostatin A was used as a reference compound. The results were summarized as IC₅₀ values in Table 2.

Table 2. Effect of compounds against as HDAC1 and HDAC4.

Comp.	HDAC1 IC ₅₀ (µg/mL)	HDAC4 IC ₅₀ (µg/mL)
5a	1.34	5.27
5b	1.01	7.99
5f	1.90	5.82
5i	0.15	8.311
5k	0.23	6.45
5m	0.05	2.83
Trichostatin A	0.03	3.35

In general, as appeared in Table 2, the synthesized compounds have higher selectivity towards HDAC1 than HDAC4. These results match the reported behavior of uracil derivatives against HDAC1 [40].

Regarding the HDAC1 inhibitory activity, compound **5m** was the most potent member (IC₅₀ = 0.05 µg/mL) compared to trichostatin A (IC₅₀ = 0.035 µg/mL). In addition, compounds **5i** and **5k** showed strong activities with IC₅₀ values of 0.146 and 0.23 µg/mL, respectively. Furthermore, compounds **5a**, **5b**, and **5f** showed moderate HDAC1 inhibitory activities with IC₅₀ values of 1.34, 1.01, and 1.9 µg/mL, respectively.

For HDAC4 inhibitory activity, compound **5m** showed superior activity (IC₅₀ = 2.83 µg/mL) than trichostatin A (IC₅₀ = 3.35 µg/mL). In addition, compounds **5a**, **5b**, **5f**, **5i**, and **5k** showed moderate HDAC4 inhibitory activities with IC₅₀ values ranging from 5.27 to 8.311 µg/mL.

2.2.4. Cell Cycle Analysis

The effect of the most promising compound, **5m**, against the cell cycle was tested in HCT116 cells. The tested cells were subjected to compound **5m** with a concentration of 78 µM (IC₅₀ value of compound **5m**) after 72 h. As presented in Table 3 and Figure 5, the percent of HCT-116 treated cells increased at the %G0–G1 phase (55.31) compared to its concentration in the control cells (43.82%). On the contrary, the percentage of HCT-116 cells decreased at the S phase from 41.19 to 34.88%. Similarly, it decreased at the G2/M phase from 15.04% to 9.81%. Such findings revealed that compound **5m** arrested the HCT-116 cell growth at G0–G1 phase.

Table 3. Effect of compound **5m** on stages of the cell death process in HCT-116 cells after 72 h treatment.

Sample	%G0–G1	%S	%G2/M
5m/HCT116	55.31	34.88	9.81
Cont. HCT116	43.82	41.16	15.02

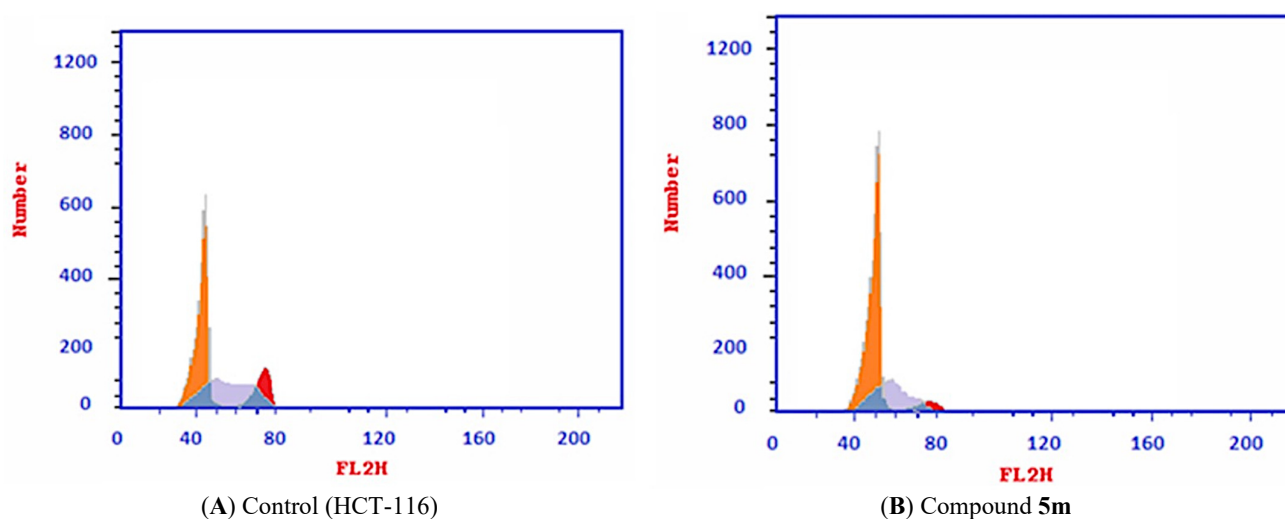


Figure 5. Flow cytometric analysis of cell cycle phases posts compounds **5m** treatment. (A) The representative histograms show the cell cycle distribution of control (HCT-116). (B) HCT-116 cells treated with compound **5m**.

2.2.5. Apoptosis Analysis

Compound **5m** was tested for apoptotic effect in HCT-116 using Annexin-V/propidium iodide (PI) staining assay. The tested cells were subjected to 78 μM from compound **5m** with an incubation time of 72 h. The results revealed that the apoptotic effect of compound **5m** was almost 17 times (37.59%) more than observed in control cells (2.17%). The early apoptosis increased from 0.43% to 22.36%. The late apoptosis increased from 0.18 to 13.14% (Table 4 and Supplementary data).

Table 4. Apoptotic effect of compound **5m** on HCT-116 cells after 72 h treatment.

Sample	DNA Content (%) ^a			Necrosis
	Total	Early	Late	
Treated HCT116 with 5m	37.59	22.36	13.14	2.09
Untreated HCT116	2.17	0.43	0.18	1.56

^a Values are reported as the mean of three different experiments.

2.2.6. Caspase-3 and Caspase-8 Determination

Due to the potential effect of both caspase-3 and caspase-8 on the apoptosis pathway [41], the effects of the most active candidate **5m** on the level of caspase-3 and caspase-8 were tested on HCT-116 72 h. As shown in Table 5, Compound **5m** showed significant increases in the levels of caspase-3 and caspase-8 (5- and 2.5-fold, respectively) compared to the control cells. Taking Staurosporine as a positive control, compound **5m** showed slightly less activity against the level of caspase-3 and caspase-8, as deduced from Table 5.

2.2.7. Cytotoxicity against Normal Cell Line

The cytotoxicity of the most promising candidate, **5m** against normal cells (WI-38), was assessed using an MTT assay. Staurosporine was used as a reference molecule. The results are summarized in Table 1.

The results revealed that compound **5m** has very low cytotoxicity against WI-38 cells with an IC_{50} value of 65.67 μM compared with Staurosporine ($\text{IC}_{50} = 51.48 \mu\text{M}$). The obtained results indicated that compound **5m** is safer than Staurosporine.

Table 5. Effect of compound **5m** on the level of caspase-3 and caspase-8 in HCT-116 cells after 72 h treatment.

Sample ID and Treatment	RT-PCR (Fold Change)	
	Caspase-3	Caspase-8
Treated HCT116 with 5m	4.891	2.655
Treated HCT116 with Staurosporine	6.8073	3.4529
Untreated HCT116	1	1

2.3. Docking Studies

All the synthesized compounds were docked against the crystal structure of HDAC1 (PDB ID: 1C3R) using MOE2019 software to reach a good insight into their binding pattern. Trichostatin A (The co-crystallized ligand) was utilized as a reference molecule. The binding pattern of some examples is presented below. The binding free energies (ΔG) for all the target molecules against HDAC1 are shown in Table 6.

Table 6. Binding free energies (ΔG in Kcal/mol) of the synthesized compounds and trichostatin A against HDAC1.

Comp.	Binding Energy	Comp.	Binding Energy
5a	−17.21	5l	−15.43
5b	−14.13	5m	−14.99
5c	−16.16	6a	−12.57
5d	−14.72	6b	−13.81
5e	−16.76	6c	−15.75
5f	−17.16	6d	−17.51
5g	−17.48	7a	−12.99
5h	−17.49	7b	−15.06
5i	−17.35	7c	−14.13
5j	−20.48	Trichostatin A	−19.11
5k	−15.36		

Trichostatin A exhibited a binding score of −19.11 kcal/mol against HDAC1. The hydroxamic acid group occupied the zinc-binding region forming many hydrogen bonds with Gly140 and Tyr297. Also, the hydroxamic acid group was involved in an electrostatic interaction with zinc ions. Three hydrophobic bonds were formed between the linker chain and Leu265, Phe198, and His170. The surface recognition motif was occupied by the *N,N*-dimethylaniline moiety (Figure 6).

Compound **5b** exhibited a binding mode like that of Trichostatin A, with a binding score of −14.13 kcal/mol. One of the two 6-amino-1-ethyl-2-thioxo-2,3-dihydropyrimidin-4(1*H*)-one moieties occupied the zinc-binding region forming one hydrogen bond with His131. Such moiety formed three electrostatic bonds with Zn ion, Tyr297, and His132, and two hydrophobic bonds with Phe198 and His132. The chlorobenzene moiety occupied the linker region forming two hydrophobic interactions with Leu265 and Tyr196. The other 6-amino-1-ethyl-2-thioxo-2,3-dihydropyrimidin-4(1*H*)-one moiety occupied the surface recognition region forming one hydrophobic interaction with Leu265 (Figure 7).

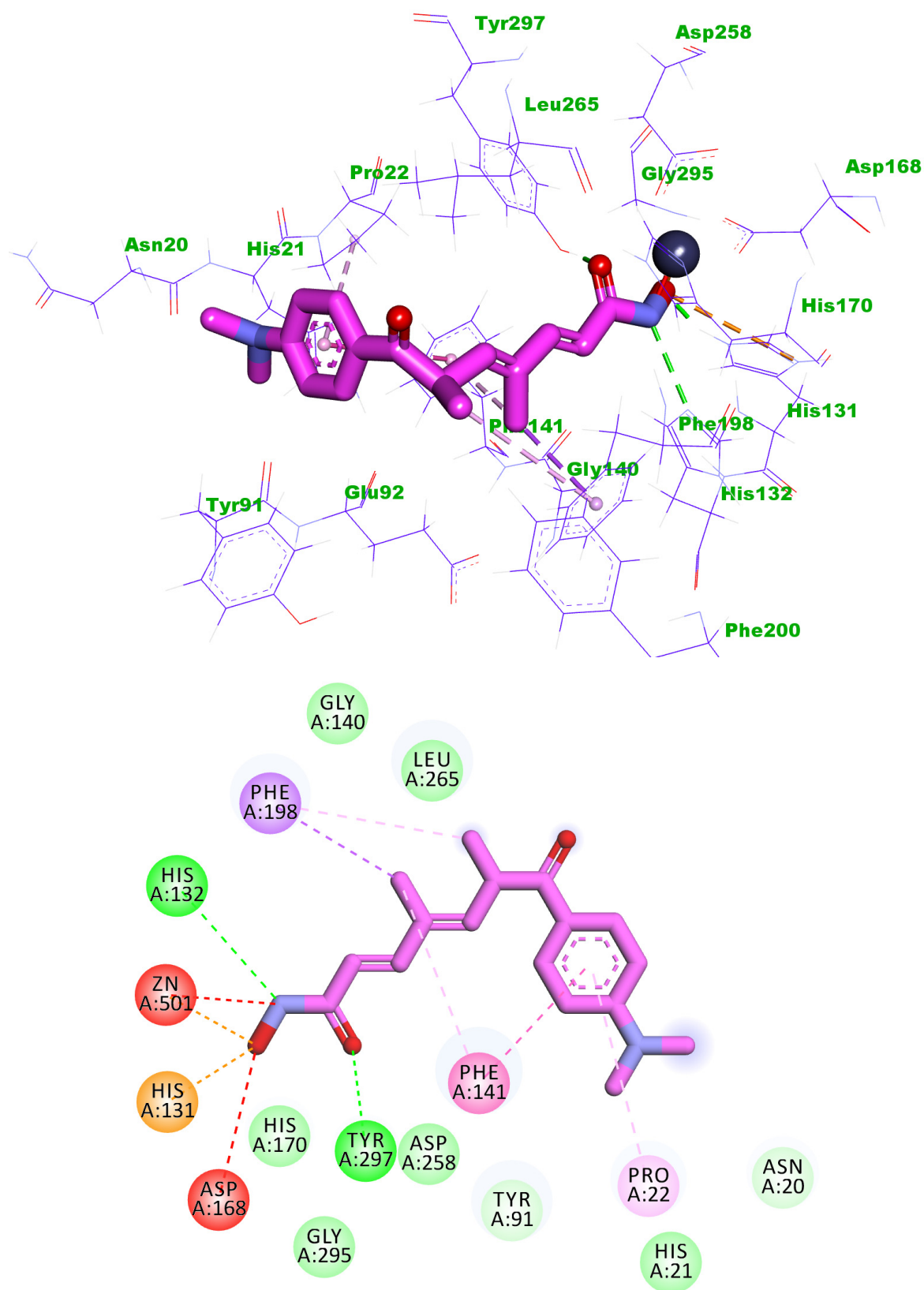


Figure 6. The Predicted binding mode of Trichostatin A with the active site of HDAC1.

Compound **5i** showed a binding energy of -17.35 kcal/mol. The first 6-amino-1-propylpyrimidine-2,4(1*H*,3*H*)-dione moiety occupied the zinc binding region forming two hydrogen bonds with His131 and Asp258. In addition, it formed three electrostatic bonds

with Zn ion and His132. Also, it formed two hydrophobic bonds with Cys142 and Leu23. The phenyl moiety occupied the linker region. The other 6-amino-1-propylpyrimidine-2,4(1*H*,3*H*)-dione moiety occupied the surface recognition region forming one hydrogen bond and one hydrophobic interaction with Leu265 (Figure 8).

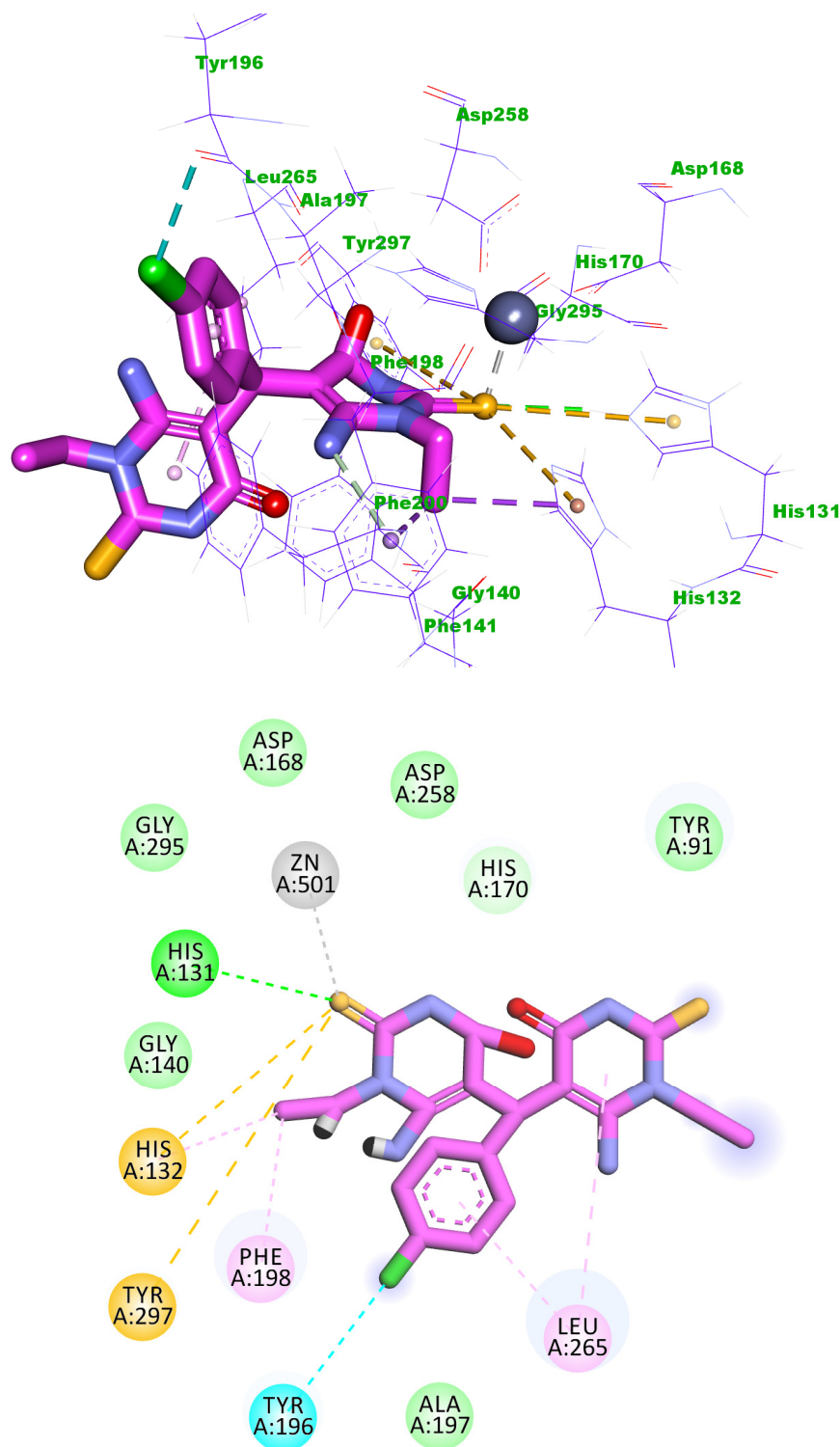


Figure 7. Predicted binding mode of compound **5b** with the active sites of HDAC1.

Compound **5k** showed a binding energy of -15.36 kcal/mol. One 6-amino-1-propylpyrimidine-2,4(1*H*,3*H*)-dione moiety was oriented into the zinc binding region, forming one hydrogen

bond with Tyr297. Three electrostatic interactions were formed between the first 6-amino-1-propylpyrimidine-2,4(1*H*,3*H*)-dione moiety and Zn ion, His170, and Phe141. Also, it formed three hydrophobic interactions with Phe141, Phe198, and His132. The central tolyl moiety occupied the linker region forming a hydrophobic interaction with Phe200. The other 6-amino-1-propylpyrimidine-2,4(1*H*,3*H*)-dione moiety occupied the surface recognition region forming three hydrophobic interactions with Leu265, Pro22, and Phe141 (Figure 9).

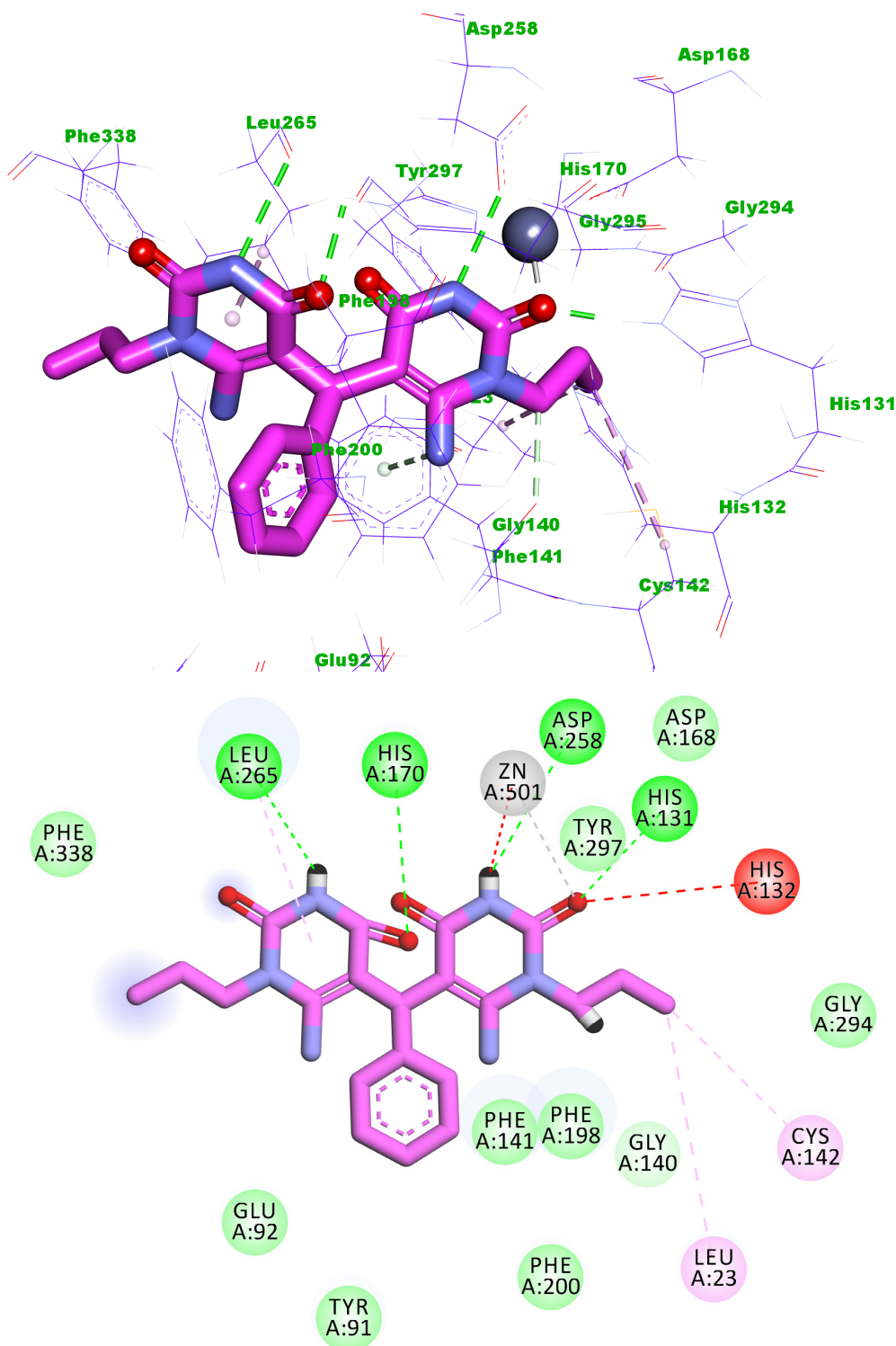


Figure 8. Predicted binding mode of compound 5i with the active site of HDAC1.

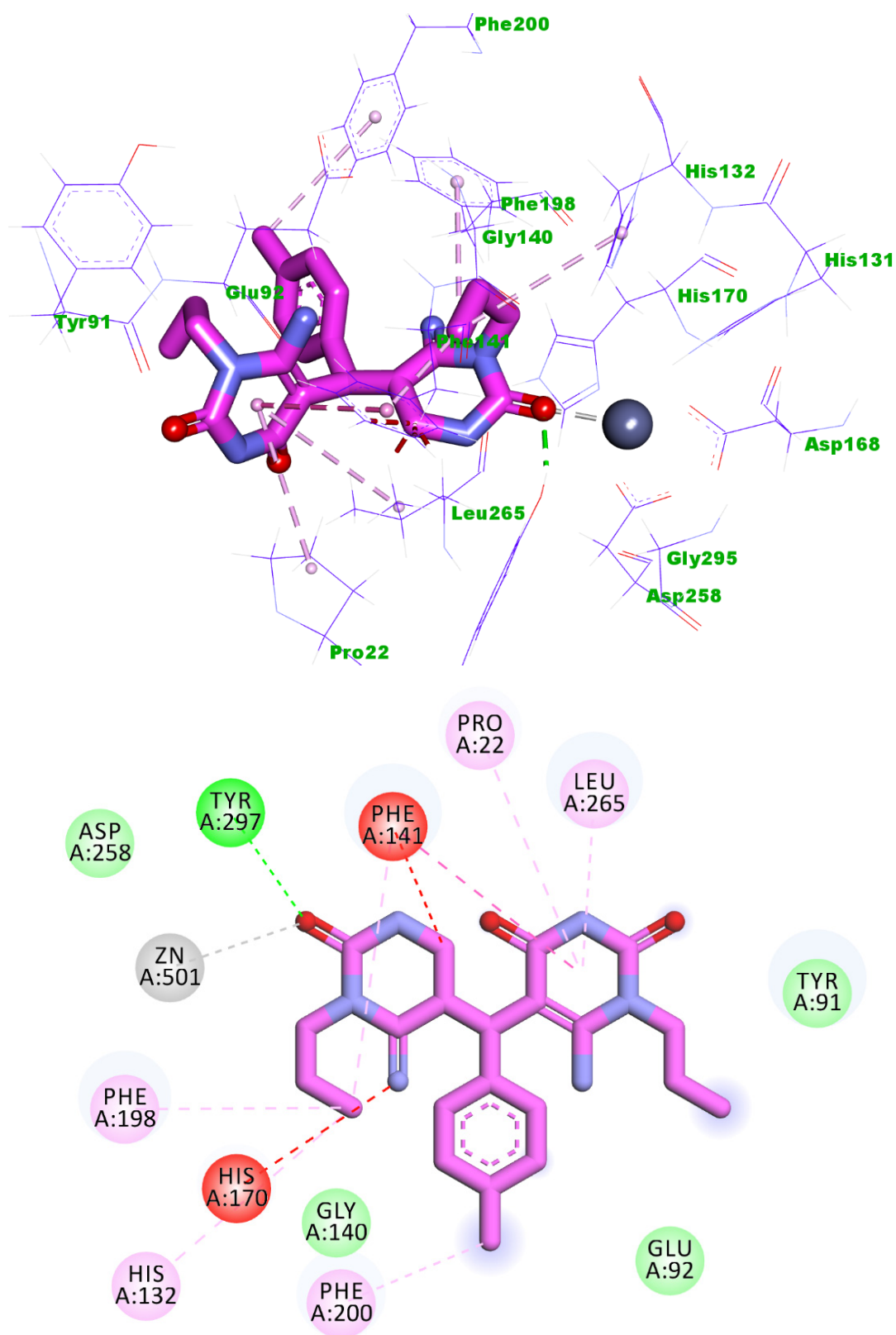


Figure 9. Predicted binding mode of compound 5k with the active site of HDAC1.

Compound 5m showed a binding energy of -14.99 kcal/mol. The first 6-amino-1-propylpyrimidine-2,4(1*H*,3*H*)-dione moiety occupied the zinc binding region forming two hydrogen bonds with Tyr297 and His170. In addition, it formed four electrostatic

interactions with Zn ion, Leu265, Gly140, and Phe198. Also, it formed four hydrophobic interactions with Phe141, Phe198, Leu265, and His132. The central 4-chlorophenyl moiety occupied the linker region forming a hydrophobic interaction with Leu265. The other 6-amino-1-propylpyrimidine-2,4(1*H*,3*H*)-dione moiety occupied the surface recognition region forming two hydrophobic interactions with Tyr91 and Phe198. In addition, it formed a hydrogen bond with Tyr91 (Figure 10).

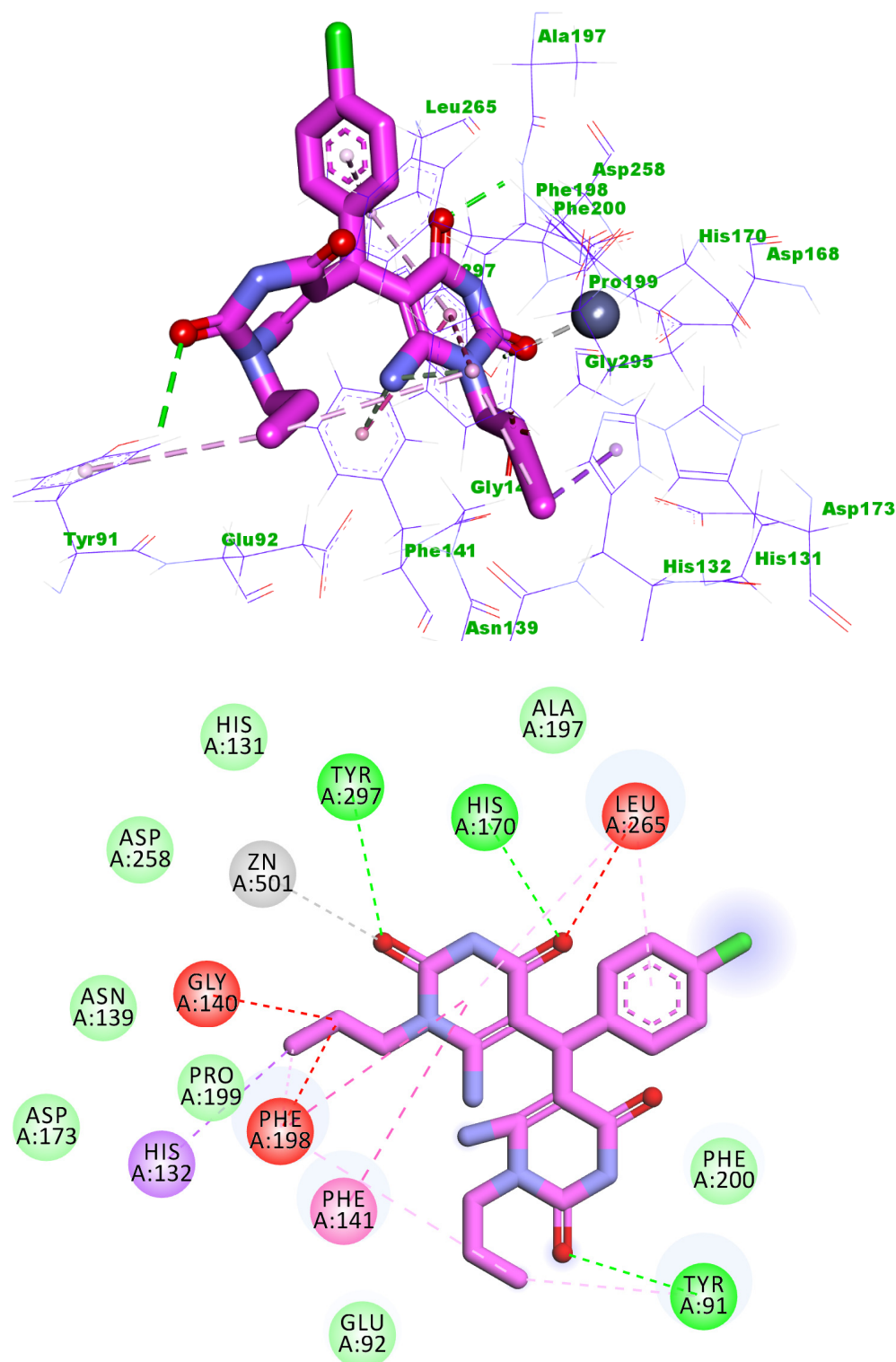


Figure 10. Predicted binding mode of compound **5m** with the active site of HDAC1.

3. Conclusions

Twenty uracil and thiouracil derivatives were synthesized as potential inhibitors for HDAC. These compounds were tested for their cytotoxic effect against MCF-7, HepG2, and HCT-116 cell lines. Some compounds showed promising anti-proliferative activities. **5a**, **5b**, and **5f**, has promising anti-proliferative effect against MCF-7 with IC₅₀ values of 11 ± 1.6, 55 ± 2.8, 9.3 ± 3.4 μM, respectively compared to sorafenib (IC₅₀ = 141 ± 3 μM). In addition, compound **5b** showed high activity against HCT-116 cells with an IC₅₀ value of 21 ± 2.4 μM compared to sorafenib (IC₅₀ = 177 ± 0.93 μM). Furthermore, compounds **5i**, **5k**, and **5m** exhibited high cytotoxic effect against HepG2 with IC₅₀ values of 4 ± 1, 5 ± 2, and 3.3 ± 0.56 μM, respectively, compared to sorafenib (IC₅₀ = 17 ± 2.3 μM). SAR study revealed that the synthesized compounds with open chain linkers (**5a–m**) are more active than that with cyclic linkers (**6a–d**, and **7a–c**). Compound **5m** showed an IC₅₀ of 0.05 μg/mL against HDAC1 compared to trichostatin A (IC₅₀ = 0.0349 μg/mL). Furthermore, compound **5m** showed superior activity (IC₅₀ = 2.83 μg/mL) than trichostatin A (IC₅₀ = 3.349 μg/mL) against HDAC4. The most promising compound **5m** arrested the HCT-116 cell growth at the G0-G1 phase and induced apoptosis by 17-fold compared to the control. In addition, such a compound increased the levels of caspase-3 and caspase-8 in HCT-116 cells. Finally, the docking studies indicated that the synthesized compounds have a binding mode almost like the reference molecule (trichostatin A) against the prospective target (HDAC).

4. Experimental

4.1. Chemistry

4.1.1. General

All advice used in the synthesis and analysis of the new compounds was presented in Supplementary data.

4.1.2. 6-Amino-1-alkyl-2-oxo/thioxo-2,3-dihydropyrimidinones (**3a,b**)

It was prepared according to the reported method [29–34].

4.1.3. 5,5'-(Arylmethylene)bis(6-amino-1-alkyl-2-oxo/thioxo-2,3-dihydropyrimidinones) (**5a–m**)

A mixture of compounds 6-aminouracil and/or thiouracil (**3a** and/or **3b**) (2.0 mmol) and different appropriate aromatic aldehydes (1.0 mmol) (**4a–h**) in the presence of conc. hydrochloric acid as a catalyst in absolute ethanol (20 mL) was stirred at room temperature for 2–3 h. The formed precipitate was collected by filtration, washed with methanol, and recrystallized from DMF:ethanol (3:1) afforded the desired compounds (**5a–m**) in good yields (Scheme 1). The structures of the synthesized compounds were confirmed by ¹H and ¹³C NMR spectroscopy.

5,5'-(Phenylmethylene)bis(6-amino-1-ethyl-2-thioxo-2,3-dihydropyrimidin-4(1H)-one) (**5a**)

White Solid, (yield: 77%), m.p. > 300 °C; HPLC (99.65%); IR (KBr) cm⁻¹: 3390, 3102 (NH₂, NH), 3050 (CH arom.), 2972, 2927 (CH aliph.), 1636 (C=O), 1520 (C=C); ¹H NMR (400 MHz, DMSO-d₆) δ 12.25 (s, 2H, 2NH, exchangeable with D₂O), 7.70 (s, 4H, NH₂, exchangeable with D₂O), 7.23 (t, J = 7.5 Hz, 2H, arom.), 7.12 (t, J = 7.5 Hz, 1H, arom.), 7.07 (d, J = 7.6 Hz, 2H, arom.), 5.51 (s, 1H, CH-5), 4.62–4.30 (m, 4H, 2CH₂), 1.22 (t, J = 6.7 Hz, 6H, 2CH₃); ¹³C NMR (100 MHz, DMSO-d₆) δ 174.71, 161.44, 154.62, 138.51, 128.33, 126.89, 125.72, 91.29, 43.64, 34.92, 12.37; MS (70 eV) m/z (%): 430 (M⁺, 5), 258 (16), 102 (31), 44 (100); Anal. Calcd for C₁₉H₂₂N₆O₂S₂ (430.55): C, 53.00; H, 5.15; N, 19.52; Found: C, 53.19; H, 5.39; N, 19.78.

5,5'-(p-Tolylmethylene)bis(6-amino-1-ethyl-2-thioxo-2,3-dihydropyrimidin-4(1H)-one) (**5b**)

White solid, (yield: 63%), m.p. = 239–240 °C; HPLC (99.65%); IR (KBr) cm⁻¹: 3376, 3158 (NH₂, NH), 3070 (CH arom.), 2976, 2928 (CH aliph.), 1661 (C=O), 1565 (C=C), 833 (p-substituted phenyl); ¹H NMR (400 MHz, DMSO-d₆) δ 12.42 (s, 2H, NH), 8.04 (d, J = 8.2 Hz,

2H, arom.), 7.34 (m, 2H, arom.), 7.05 (s, 4H, 2NH₂), 6.05 (s, 1H, CH-5), 4.58 (q, *J* = 6.9 Hz, 2H, CH₂), 4.30 (q, *J* = 6.8 Hz, 2H, CH₂), 2.38 (s, 3H, CH₃), 1.34 (t, *J* = 6.9 Hz, 3H, CH₃), 1.13 (t, *J* = 6.8 Hz, 3H, CH₃); ¹³C NMR (100 MHz, DMSO-*d*₆) δ 172.90, 161.91, 152.27, 140.52, 129.59, 128.67, 128.25, 127.81, 126.58, 94.32, 42.78, 32.93, 21.01, 12.13; MS (70 eV) *m/z* (%): 444 (M⁺, 39), 375 (44), 274 (100), 169 (50), 62 (39); Anal. Calcd for C₂₀H₂₄N₆O₂S₂ (444.57): C, 54.03; H, 5.44; N, 18.90; Found: C, 54.21; H, 5.67; N, 19.08.

5,5'-((4-Chlorophenyl)methylene)bis(6-amino-1-ethyl-2-thioxo-2,3-dihydropyrimidin-4(1H)-one) (5c)

White solid, (yield: 78%), m.p. > 300 °C; IR (KBr) cm⁻¹: 3376, 3153 (NH₂, NH), 3050 (CH arom.), 2976, 2928 (CH aliph.), 1661 (C=O), 1565 (C=C), 839 (*p*-substituted phenyl); ¹H NMR (400 MHz, DMSO-*d*₆) δ 12.28 (s, 2H, 2NH), 7.69 (s, 4H, 2NH₂), 7.27 (d, *J* = 8.5 Hz, 2H, arom.), 7.10 (d, *J* = 8.5 Hz, 2H, arom.), 5.48 (s, 1H, CH-5), 4.57-4.36 (m, 4H, 2CH₂), 1.23 (t, *J* = 6.7 Hz, 6H, 2CH₃); ¹³C NMR (100 MHz, DMSO-*d*₆) δ 174.29, 164.21, 158.52, 137.26, 129.77, 128.48, 127.71, 87.32, 43.19, 34.08, 11.90; MS (70 eV) *m/z* (%): 466 (M⁺, 4), 464 (M⁺, 10), 333 (12), 292 (95), 190 (20), 44 (100); Anal. Calcd for C₁₉H₂₁ClN₆O₂S₂ (464.99): C, 49.08; H, 4.55; N, 18.07; Found: C, 49.32; H, 4.69; N, 18.23.

5,5'-((2,4-Dichlorophenyl)methylene)bis(6-amino-1-ethyl-2-thioxo-2,3-dihydro pyrimidin-4(1H)-one) (5d)

White powder (yield: 60%), m.p. = 272–273 °C; IR (KBr) cm⁻¹: 3373, 3145 (NH₂, NH), 3065 (CH arom.), 2975, 2931 (CH aliph.), 1663 (C=O), 1572 (C=C), 730 (trisubstituted phenyl); ¹H NMR (400 MHz, DMSO-*d*₆) δ 12.29 (s, 2H, 2NH), 7.75 (s, 2H, NH₂), 7.46 (d, *J* = 1.7 Hz, 1H, arom.), 7.33 (dd, *J* = 8.5, 1.7 Hz, 1H, arom.), 7.28 (d, *J* = 8.5 Hz, 1H, arom.), 7.16 (s, 2H, NH₂), 5.41 (s, 1H, CH-5), 4.45 (m, 4H, 2CH₂), 1.22 (t, *J* = 6.8 Hz, 6H, 2CH₃). ¹³C NMR (100 MHz, DMSO-*d*₆) δ 174.26, 164.18, 153.87, 136.32, 133.15, 131.04, 130.17, 128.90, 126.71, 90.57, 43.24, 33.55, 11.89; MS (70 eV) *m/z* (%): 503 (M⁺, 23), 501 (M⁺, 26), 499 (M⁺, 35), 360 (100), 300 (31), 286 (42), 255 (18); Anal. Calcd for C₁₉H₂₀Cl₂N₆O₂S₂ (499.43): C, 45.69; H, 4.04; N, 16.83; Found: C, 45.78; H, 4.21; N, 17.05.

5,5'-((4-Methoxyphenyl)methylene)bis(6-amino-1-ethyl-2-thioxo-2,3-dihydropyrimidin-4(1H)-one) (5e)

White powder (yield: 67%), m.p. = 260–261 °C; ¹H NMR (400 MHz, DMSO-*d*₆) δ 12.22 (s, 2H, 2NH), 7.95 (s, 2H, NH₂), 7.74 (s, 2H, NH₂), 6.96 (d, *J* = 8.6 Hz, 2H, arom.), 6.79 (d, *J* = 8.6 Hz, 2H, arom.), 5.45 (s, 1H, CH-5), 4.45 (m, 4H, 2CH₂), 3.70 (s, 3H, OCH₃), 1.22 (t, *J* = 6.8 Hz, 6H, 2CH₃); ¹³C NMR (100 MHz, DMSO-*d*₆) δ 174.20, 162.32, 157.06, 153.88, 129.64, 127.45, 113.28, 91.37, 54.94, 43.11, 35.79, 11.90; MS (70 eV) *m/z* (%): 460 (M⁺, 30), 392 (41), 222 (30), 129 (100), 56 (40); Anal. Calcd for C₂₀H₂₄N₆O₃S₂ (460.57): C, 52.16; H, 5.25; N, 18.25; Found: C, 52.40; H, 5.37; N, 18.49.

5,5'-((4-Nitrophenyl)methylene)bis(6-amino-1-ethyl-2-thioxo-2,3-dihydropyrimidin-4(1H)-one) (5f)

White solid, (yield: 79%) m.p. = 274–275 °C; HPLC (99.00%); IR (KBr) cm⁻¹: 3384, 3137 (NH₂, NH), 3060 (CH arom.), 2975, 2931 (CH aliph.), 1662 (C=O), 1555 (C=C), 1505, 1344 (NO₂), 849 (*p*-substituted phenyl); ¹H NMR (400 MHz, DMSO-*d*₆) δ 12.34 (s, 2H, 2NH), 8.10 (d, *J* = 8.7 Hz, 2H, arom.), 7.69 (s, 4H, 2NH₂), 7.38 (d, *J* = 8.7 Hz, 2H, arom.), 5.58 (s, 1H, CH-5), 4.49 (m, 4H, 2CH₂), 1.23 (t, *J* = 6.8 Hz, 6H, 2CH₃); ¹³C NMR (100 MHz, DMSO-*d*₆) δ 174.42, 162.32, 154.24, 147.27, 145.44, 127.98, 123.02, 90.60, 43.26, 35.79, 11.87; MS (70 eV) *m/z* (%): 475 (M⁺, 20), 425 (71), 372 (85), 343 (100), 297 (20) Anal. Calcd for C₁₉H₂₁N₇O₄S₂ (475.54): C, 47.99; H, 4.45; N, 20.62; Found: C, 48.17; H, 4.63; N, 20.89.

5,5'-(Thiophen-2-ylmethylene)bis(6-amino-1-ethyl-2-thioxo-2,3-dihydropyrimidin-4(1H)-one) (5g)

White solid, (yield: 56%) m.p. = 271–272 °C; IR (KBr) cm⁻¹: 3380, 3142 (NH₂, NH), 3030 (CH arom.), 2976, 2924 (CH aliph.), 1630 (C=O), 1566 (C=C); ¹H NMR (400 MHz,

DMSO- d_6) δ 12.29 (s, 2H, 2NH), 7.87 (br.s, 4H, 2NH₂), 7.27 (d, 1H, arom.), 6.85 (t, 1H, arom.), 6.65 (s, 1H, arom.), 5.64 (s, 1H, CH-5), 4.50 (m, 4H, 2CH₂). 1.21 (t, $J = 6.9$ Hz, 6H, 2CH₃); ¹³C NMR (100 MHz, DMSO- d_6) δ 174.35, 162.34, 153.85, 143.73, 126.28, 123.79, 123.60, 91.51, 43.11, 18.56, 11.86; MS (70 eV) m/z (%): 436 (M⁺, 7), 264 (58), 171 (90), 44 (100); Anal. Calcd for C₁₇H₂₀N₆O₂S₃ (436.57): C, 46.77; H, 4.62; N, 19.25; Found: C, 46.98; H, 4.76; N, 19.51.

5,5'-Methylenebis(6-amino-1-propylpyrimidine-2,4(1H,3H)-dione) (5h)

White solid, (yield 49%), m.p. = 256–257 °C; IR (KBr) cm⁻¹: 3342, 3133 (NH₂, NH), 2969, 2938 (CH aliph.), 1677 (C=O), 1590 (C=C); ¹H NMR (400 MHz, DMSO- d_6) δ 11.40 (s, 1H, NH), 10.53 (s, 1H, NH), 7.52 (br. s, 2H, NH₂), 7.16 (s, 2H, NH₂), 3.64 (m, 4H, 2CH₂), 2.66 (s, 2H, CH₂), 1.50 (m, 4H, 2 CH₂), 0.85 (m, 6H, 2CH₃); ¹³C NMR (100 MHz, DMSO- d_6) δ 164.02, 161.53, 150.50, 148.84, 84.97, 80.36, 45.59, 45.23, 20.86, 20.72, 17.75, 11.10, 10.71; MS (70 eV) m/z (%): 350 (M⁺, 18), 386 (61), 220 (100), 144 (37), 61 (80); Anal. Calcd for C₁₅H₂₂N₆O₄ (350.38): C, 51.42; H, 6.33; N, 23.99; Found: C, 51.67; H, 6.45; N, 23.75.

5,5'-(Phenylmethylene)bis(6-amino-1-propylpyrimidine-2,4(1H,3H)-dione) (5i)

Pale yellow solid, yield (66%), m.p. = 294–295 °C; HPLC (99.58%); IR (KBr) cm⁻¹: 3388, 3178 (NH₂, NH), 3045 (CH arom.), 2969, 2930 (CH aliph.), 1670 (C=O), 1598 (C=C); ¹H NMR (400 MHz, DMSO- d_6) δ 10.71 (s, 2H, 2NH), 7.73–7.41 (br s, 4H, 2NH₂), 7.19 (t, $J = 7.6$ Hz, 2H, arom.), 7.07 (m, 3H, arom.), 5.45 (s, 1H, CH-5), 3.77 (m, 4H, 2CH₂), 1.56 (m, 4H, 2CH₂), 0.88 (t, $J = 7.4$ Hz, 6H, 2CH₃); ¹³C NMR (100 MHz, DMSO- d_6) δ 150.08, 139.67, 134.59, 129.49, 129.16, 127.63, 126.44, 124.84, 71.90, 42.78, 34.13, 20.70, 10.76; MS (70 eV) m/z (%): 426 (M⁺, 39), 256 (42), 215 (43), 106 (100), 40 (17); Anal. Calcd for C₂₁H₂₆N₆O₄ (426.48): C, 59.14; H, 6.15; N, 19.71; Found: C, 59.36; H, 6.29; N, 19.87.

5,5'-(*p*-Tolylmethylene)bis(6-amino-1-propylpyrimidine-2,4(1H,3H)-dione) (5j)

Pale yellow solid, (yield 73%), m.p. = 286–287 °C; IR (KBr) cm⁻¹: 3387, 3180 (NH₂, NH), 3049 (CH arom.), 2968, 2934 (CH aliph.), 1694 (C=O), 1560 (C=C), 845 (*p*-substituted phenyl); ¹H NMR (400 MHz, DMSO- d_6) δ 10.69 (s, 2H, 2NH), 7.67 (br.s, 2H, NH₂), 7.39 (br.s, 2H, NH₂), 7.00 (d, $J = 8.1$ Hz, 2H, arom.), 6.92 (d, $J = 8.1$ Hz, 2H, arom.), 5.40 (s, 1H, CH-5), 3.77 (m, 4H, 2CH₂), 2.23 (s, 3H, CH₃), 1.55 (m, 4H, 2CH₂), 0.88 (t, $J = 7.3$ Hz, 6H, 2CH₃); ¹³C NMR (100 MHz, DMSO- d_6) δ 160.73, 150.17, 145.35, 136.52, 133.64, 129.80, 129.67, 128.33, 126.43, 80.12, 42.84, 33.84, 20.76, 20.54, 10.81; MS (70 eV) m/z (%): 440 (M⁺, 27), 327 (60), 210 (62), 97 (100), 61 (86); Anal. Calcd for C₂₂H₂₈N₆O₄ (440.50): C, 59.99; H, 6.41; N, 19.08; Found: C, 60.17; H, 6.53; N, 19.31.

5,5'-((2,4-Dichlorophenyl)methylene)bis(6-amino-1-propylpyrimidine-2,4(1H,3H)-dione) (5k)

White solid, (yield 58%), m.p. 285–286 °C; HPLC (99.53%); IR (KBr) cm⁻¹: 3365, 3176 (NH, NH₂), 3049 (CH arom.), 2969, 2939 (CH aliph.), 1692 (C=O), 1568 (C=C), 709 (trisubstituted phenyl); ¹H NMR (400 MHz, d_6) δ 10.91 (s, 1H, NH), 10.66 (s, 1H, NH), 7.42 (br.s, 2H, NH₂), 7.41 (d, $J = 2.2$ Hz, 1H, arom.), 7.31 (dd, $J = 8.5, 2.2$ Hz, 1H, arom.), 7.24 (d, $J = 8.5$ Hz, 1H, arom.), 7.00 (br.s, 2H, NH₂), 5.37 (s, 1H, CH-5), 3.86–3.68 (m, 4H, 2CH₂), 1.56 (m, 4H, 2CH₂), 0.87 (t, 6H, 2CH₃); ¹³C NMR (100 MHz, DMSO) δ 163.73, 154.59, 149.93, 137.95, 133.20, 130.56, 130.19, 128.75, 126.45, 86.26, 42.80, 33.30, 20.67, 10.71; MS (70 eV) m/z (%): 499 (M⁺4, 12), 497 (M⁺2, 36), 495 (M⁺, 13), 345 (100), 257 (57), 135 (66), 59 (66); Anal. Calcd for C₂₁H₂₄Cl₂N₆O₄ (495.36): C, 50.92; H, 4.88; N, 16.97; Found: C, 51.14; H, 4.95; N, 17.13.

5,5'-((4-Methoxyphenyl)methylene)bis(6-amino-1-propylpyrimidine-2,4(1H,3H)-dione) (5l)

White solid, (yield 64%), m.p. = 289–290 °C; IR (KBr) cm⁻¹: 3376, 3150 (NH, NH₂), 3042 (CH arom.), 2963, 2923 (CH aliph.), 1688 (C=O), 1598 (C=C), 843 (*p*-substituted phenyl); ¹H NMR (400 MHz, DMSO- d_6) δ 10.78 (s, 1H, NH), 10.62 (s, 1H, NH), 7.87 (d, $J = 8.5$ Hz, 1H, arom.), 7.65 (br.s, 2H, NH₂), 7.37 (br.s, 2H, NH₂), 7.13 (d, $J = 8.5$ Hz, 1H, arom.), 6.94 (d, $J = 8.5$ Hz, 1H, arom.), 6.76 (d, $J = 8.5$ Hz, 1H, arom.), 5.39 (s, 1H, CH-5), 3.83 (m, 4H, 2CH₂),

3.69 (s, 3H, O-CH₃), 1.54 (m, 4H, 2CH₂), 0.88 (t, *J* = 7.2 Hz, 6H, 2CH₃); ¹³C NMR (100 MHz, DMSO-*d*₆) δ 164.70, 157.26, 150.57, 132.28, 131.76, 130.13, 127.89, 114.99, 113.54, 87.41, 56.17, 55.38, 43.24, 33.86, 21.18, 11.23. MS (70 eV) *m/z* (%): 456 (M⁺, 42), 306 (86), 231 (88), 191 (100), 57 (36); Anal. Calcd for C₂₂H₂₈N₆O₅ (456.50): C, 57.88; H, 6.18; N, 18.41; Found: C, 58.09; H, 6.40; N, 18.49.

5,5'-((4-Chlorophenyl)methylene)bis(6-amino-1-propylpyrimidine-2,4(1*H*,3*H*)-dione) (5m)

Pale yellow solid, yield (73%), m.p. = 257–258 °C; HPLC (99.71%); IR (KBr) cm⁻¹: 3377, 3189 (NH, NH₂), 3045 (CH arom.), 2966, 2930 (CH aliph.), 1666 (C=O), 1565 (C=C), 843 (*p*-substituted phenyl); ¹H NMR (400 MHz, DMSO-*d*₆) δ 10.81 (s, 2H, 2NH), 7.64 (br.s, 4H, 2NH₂), 7.24 (d, *J* = 8.6 Hz, 2H, arom.), 7.07 (d, *J* = 8.6 Hz, 2H, arom.), 5.42 (s, 1H, CH-5), 3.76 (m, 4H, 2CH₂), 1.56 (m, 4H, 2CH₂), 0.88 (t, *J* = 7.3 Hz, 6H, 2CH₃); ¹³C NMR (100 MHz, DMSO-*d*₆) δ 162.38, 150.10, 138.89, 128.50, 127.55, 86.57, 42.88, 35.83, 20.72, 10.80; MS (70 eV) *m/z* (%): 462 (M⁺2, 34), 460 (M⁺, 39), 385 (51), 370 (100), 269 (42), 102 (40); Anal. Calcd for C₂₁H₂₅ClN₆O₄ (460.92): C, 54.72; H, 5.47; N, 18.23; Found: C, 54.95; H, 5.63; N, 18.50.

4.1.4. 1,9-Dialkyl-2,3,5,8,9,10-hexahydropyrido[2,3-*d*:6,5-*d'*]dipyrimidinones (6a–d)

Compounds **5a**, **5f**, **5h** or **5l** (0.7 mmol) and glacial acetic acid (5 mL) were heated under reflux in the presence of c. HCl (1 mL) for 2.5 h. After cooling, the reaction mixture was filtered off, washed with ethanol crystallized from DMF and dried in the oven.

1,9-Diethyl-5-phenyl-2,8-dithioxo-2,3,5,8,9,10-hexahydropyrido[2,3-*d*:6,5-*d'*]dipyrimidine-4,6(1*H*,7*H*)-dione (6a)

White solid, (yield 75%), m.p. = 255–256 °C; ¹H NMR (400 MHz, DMSO-*d*₆) δ 12.78 (s, 2H, NH), 7.70 (s, 1H, NH), 7.26 (t, *J* = 7.5 Hz, 2H, arom.), 7.14 (m, 3H, arom.), 5.46 (s, 1H, CH-5), 4.41–4.31 (m, 4H, 2CH₂), 1.25 (t, *J* = 7.0 Hz, 3H, CH₃), 1.19 (t, *J* = 6.9 Hz, 3H, CH₃); MS (70 eV) *m/z* (%): 413 (M⁺, 59), 352 (32), 207 (49), 157 (100), 40 (54); Anal. Calcd for C₁₉H₁₉N₅O₂S₂ (413.51): C, 55.19; H, 4.63; N, 16.94; Found: C, 55.42; H, 4.78; N, 16.89.

1,9-Diethyl-5-(4-nitrophenyl)-2,8-dithioxo-2,3,5,8,9,10-hexahydropyrido[2,3-*d*:6,5-*d'*]dipyrimidine-4,6(1*H*,7*H*)-dione (6b)

Pale yellow solid, (yield: 86%), m.p. = 251–252 °C; IR (KBr) cm⁻¹: 3137 (NH), 3070 (CH arom.), 2977, 2933 (CH aliph.), 1650 (C=O), 1519 (C=C), 1500, 1342 (NO₂), 853 (*p*-substituted phenyl); ¹H NMR (400 MHz, DMSO-*d*₆) δ 12.83 (s, 2H, 2NH), 8.17–8.06 (m, 2H, arom.), 7.77 (s, 1H, NH), 7.44 (m, 2H, arom.), 5.57 (s, 1H, CH-5), 4.52–4.35 (m, 4H, 2CH₂), 1.25 (t, *J* = 7.0 Hz, 3H, CH₃), 1.19 (t, *J* = 7.0 Hz, 3H, CH₃); ¹³C NMR (100 MHz, DMSO-*d*₆) δ 173.95, 162.27, 152.16, 147.22, 145.82, 128.00, 123.20, 92.93, 43.75, 34.65, 11.53; MS (70 eV) *m/z* (%): 458 (M⁺, 31), 343 (31), 238 (41), 139 (33), 83 (100); Anal. Calcd for C₁₉H₁₈N₆O₄S₂ (458.51): C, 49.77; H, 3.96; N, 18.33; Found: C, 49.98; H, 4.17; N, 18.59.

5-(4-Methoxyphenyl)-1,9-dipropyl-5,10-dihydropyrido[2,3-*d*:6,5-*d'*]dipyrimidine-2,4,6,8(1*H*,3*H*,7*H*,9*H*)-tetraone (6c)

Yellow solid, (yield: 62%), m.p. = 180–181 °C; IR (KBr) cm⁻¹: 3223 (NH), 3091 (CH arom.), 2962, 2937 (CH aliph.), 1647 (C=O), 1543 (C=C), 835 (*p*-substituted phenyl); ¹H NMR (400 MHz, DMSO-*d*₆) δ 11.48 (s, 1H, NH), 11.37 (s, 1H, NH), 8.35–8.27 (m, 3H, arom., NH) 7.08–7.05 (m, 2H, arom.), 5.75 (s, 1H, CH-5), 3.87 (s, 3H, CH₃), 3.76–3.71 (m, 4H, 2CH₂), 1.57–1.53 (m, 4H, 2CH₂), 0.87 (t, *J* = 7.5 Hz, 6H, 2CH₃); ¹³C NMR (101 MHz, DMSO-*d*₆) δ 163.48, 163.37, 161.42, 161.08, 155.84, 150.38, 150.32, 137.46, 125.25, 125.11, 115.55, 115.50, 113.92, 83.69, 55.69, 42.30, 41.74, 20.82, 11.19; MS (70 eV) *m/z* (%): 439 (M⁺, 27), 311 (66), 245(100), 138 (95), 75 (49); Anal. Calcd for C₂₂H₂₅N₅O₅ (439.47): C, 60.13; H, 5.73; N, 15.94; Found: C, 59.94; H, 5.91; N, 16.17.

1,9-Dipropyl-5,10-dihydropyrido[2,3-*d*:6,5-*d'*]dipyrimidine-2,4,6,8
(1*H*,3*H*,7*H*,9*H*)-tetraone (**6d**)

White solid, (yield: 70%), m.p. = 274–275 °C; IR (KBr) cm^{-1} : 3233 (NH), 2969, 2938 (CH aliph.), 1677 (C=O), 1589 (C=C); ^1H NMR (400 MHz, DMSO- d_6) δ 11.40 (s, 1H, NH), 10.53 (s, 1H, NH), 7.18 (s, 1H, NH), 3.74–3.60 (m, 4H, 2CH₂), 3.49 (s, 2H, CH₂), 1.56–1.44 (m, 4H, 2 CH₂), 0.86 (t, J = 5.0 Hz, 3H, CH₃), 0.83 (t, J = 5.1 Hz, 3H, CH₃); ^{13}C NMR (100 MHz, DMSO- d_6) δ 161.55, 150.51, 150.29, 148.87, 80.37, 45.62, 45.26, 27.70, 20.88, 20.74, 11.11, 10.73; MS (70 eV) m/z (%): 333 (M⁺, 42), 215 (70), 185 (100), 84 (66); Anal. Calcd for C₁₅H₁₉N₅O₄ (333.35): C, 54.05; H, 5.75; N, 21.01; Found: C, 54.21; H, 5.89; N, 20.96.

4.1.5. 5Aryl-1,9-Diethyl-2,8-dithioxo-2,3,8,9-tetrahydropyrido[2,3-*d*:6,5-*d'*]dipyrimidine-4,6(1*H*,7*H*)-diones (**7a–c**)

A mixture of compound **5c**, **5e** or **5g** (0.7 mmol), glacial acetic acid (5 mL) and c. HCl (1 mL) was heated under reflux for 4–5 h. After cooling, the formed precipitate was collected by filtration, washed with ethanol crystallized from DMF and dried in the oven.

5-(4-Chlorophenyl)-1,9-diethyl-2,8-dithioxo-2,3,8,9-tetrahydropyrido[2,3-*d*:6,5-*d'*]dipyrimidine-4,6(1*H*,7*H*)-dione (**7a**)

Yellow solid, (yield: 72%), m.p. = 224–225 °C; IR (KBr) cm^{-1} : 3229 (NH), 3109 (CH arom.), 2976, 2928 (CH aliph.), 1662 (C=O), 1572 (C=C), 834 (*p*-substituted phenyl); ^1H NMR (400 MHz, DMSO- d_6) δ 10.01 (s, 2H, 2NH), 7.93 (d, J = 8.5 Hz, 2H, arom.), 7.68 (d, J = 8.5 Hz, 2H, arom.), 4.32–4.22 (m, 2H, CH₂), 4.12–4.05 (m, 2H, CH₂), 1.30–1.10 (m, 6H, 2CH₃); MS (70 eV) m/z (%): 448 (M⁺2, 6), 446 (M⁺, 17), 402 (77), 325 (100), 249 (54), 69 (22); Anal. Calcd for C₁₉H₁₆ClN₅O₂S₂ (445.94): C, 51.17; H, 3.62; N, 15.71; Found: C, 51.37; H, 3.76; N, 15.92.

1,9-Diethyl-5-(4-methoxyphenyl)-2,8-dithioxo-2,3,8,9-tetrahydropyrido[2,3-*d*:6,5-*d'*]dipyrimidine-4,6(1*H*,7*H*)-dione (**7b**)

Mustard yellow, yield (66%), m.p. = 221–221 °C; IR (KBr) cm^{-1} : 3235 (NH), 3070 (CH arom.), 2988, 2935 (CH aliph.), 1660 (C=O), 1569 (C=C), 843 (*p*-substituted phenyl); ^1H NMR (400 MHz, DMSO- d_6) δ 12.47 (s, 1H, NH), 12.40 (s, 1H, NH), 8.43 (d, J = 9.0 Hz, 1H, arom.), 8.31 (d, J = 9.0 Hz, 1H, arom.), 7.10–7.07 (m, 2H, arom.), 4.32 (q, J = 6.9 Hz, 4H, 2 CH₂), 3.89 (s, 3H, CH₃), 1.18 (t, J = 6.9 Hz, 6H, 2CH₃); ^{13}C NMR (100 MHz, DMSO- d_6) δ 178.64, 178.57, 164.23, 164.10, 162.52, 157.35, 156.82, 156.67, 131.82, 129.66, 127.46, 114.53, 114.14, 113.12, 55.82, 55.70, 54.89, 12.34, 12.26; MS (70 eV) m/z (%): 441 (M⁺, 18), 355 (41), 235 (100), 113 (28), 50 (39); Anal. Calcd for C₂₀H₁₉N₅O₃S₂ (441.52): C, 54.41; H, 4.34; N, 15.86; Found: C, 54.21; H, 4.51; N, 16.04.

1,9-Diethyl-5-(thiophen-2-yl)-2,8-dithioxo-2,3,8,9-tetrahydropyrido[2,3-*d*:6,5-*d'*]dipyrimidine-4,6(1*H*,7*H*)-dione (**7c**)

Brown solid, (yield: 54%), m.p. = 216–217 °C; IR (KBr) cm^{-1} : 3207 (NH), 3050 (CH arom.), 2972, 2926 (CH aliph.), 1657 (C=O), 1568 (C=C); ^1H NMR (400 MHz, DMSO- d_6) δ 12.50 (s, 2H, 2NH), 8.38 (t, 1H, arom.), 8.27 (t, 1H, arom.), 7.41 (m, 1H, arom.), 4.34 (m, 4H, 2CH₂), 1.17 (m, 6H, 2CH₃); ^{13}C NMR (100 MHz, DMSO- d_6) δ 178.59, 178.55, 161.36, 160.34, 160.21, 159.38, 143.60, 136.87, 128.88, 128.79, 111.98, 100.93, 54.86, 48.17, 14.51, 12.27; MS (70 eV) m/z (%): 417 (M⁺, 37), 399 (100), 298 (25), 122 (58), 44 (40); Anal. Calcd for C₁₇H₁₅N₅O₂S₃ (417.52): C, 48.90; H, 3.62; N, 16.77; Found: C, 49.08; H, 3.80; N, 16.98.

4.2. Biological Testing

4.2.1. In Vitro Cytotoxic Activity

Anti-proliferative activity activities were tested using MTT assay [36,42–45] as described in Supplementary Materials.

4.2.2. In vitro HDAC Assay

Compounds **5a**, **5b**, **5f**, **5i**, **5k**, and **5m** were tested for their HDAC inhibitory activities (HDAC1 and HDAC4 subtypes) as described in Supplementary Materials [46,47].

4.2.3. Flow Cytometry Analysis for Cell Cycle

Cell cycle analysis was performed for compound **5m** as described in Supplementary Materials [48–50].

4.2.4. Flow Cytometry Analysis for Apoptosis

The apoptotic effect of the compound **5m** was tested as described in Supplementary data [51–53]. Quantitative Real-Time Reverse-Transcriptase PCR (qRT-PCR) technique Using qRT-PCR, the effect of compound **5m** on the expression of cleaved caspase-3 and caspase-8 was determined (Supplementary Materials) [54–58].

4.3. Docking Studies

Docking studies were conducted against HDAC1 (<http://www.rcsb.org/> accessed on 1 January 2023, PDB code: 1C3R, resolution of 2.00 Å) as described in Supplementary Materials [59].

Supplementary Materials: The following supporting information can be downloaded at: <https://www.mdpi.com/article/10.3390/ph16070966/s1>, S1: chemistry, S2: Methods of biological testing, S3: docking procedure, Figures in S4: the spectral data (1H NMR, 13C NMR, Mass, and IR spectra) of the synthesized compounds, and Figures in S5: the HPLC reports [60].

Author Contributions: Conceptualization, S.E.-K. and M.H. (Mohamed Hagrass); methodology, O.R.E., M.A.E.D., M.H. (Maghawry Hegazy), A.A.E.-H., M.M.M. and S.Y.E.; software, I.H.E.; validation, I.H.E. and S.E.-K.; formal analysis M.H. (Maghawry Hegazy), M.A.E.D. and F.A.; investigation, S.E.-K. and M.H. (Mohamed Hagrass); resources, S.E.-K. and M.H. (Mohamed Hagrass); data curation, S.E.-K. and M.H. (Mohamed Hagrass); writing—original draft preparation, S.E.-K., M.A.E.D. and M.H. (Maghawry Hegazy); writing—review and editing, I.H.E. and S.E.-K.; visualization, F.A.; supervision, M.H. (Mohamed Hagrass), M.A.E.D. and S.E.-K.; project administration, S.E.-K.; funding acquisition, F.A. All authors have read and agreed to the published version of the manuscript.

Funding: This paper is based on work supported by Science, Technology & Innovation Funding Authority (STDF) under grant number (43229) young researcher.

Institutional Review Board Statement: Not applicable.

Informed Consent Statement: Not applicable.

Data Availability Statement: Not applicable.

Conflicts of Interest: The authors declare no conflict of interest.

Sample Availability: Samples of the compounds are available from the authors.

References

1. Sung, H.; Ferlay, J.; Siegel, R.L.; Laversanne, M.; Soerjomataram, I.; Jemal, A.; Bray, F. Global Cancer Statistics 2020: GLOBOCAN Estimates of Incidence and Mortality Worldwide for 36 Cancers in 185 Countries. *CA Cancer J. Clin.* **2021**, *71*, 209–249. [CrossRef]
2. WHO. Cancer. Available online: https://www.who.int/health-topics/cancer#tab=tab_1 (accessed on 1 October 2020).
3. Badran, M.M.; Abouzid, K.A.M.; Hussein, M.H.M. Synthesis of certain substituted quinoxalines as antimicrobial agents (Part II). *Arch. Pharmacol. Res.* **2003**, *26*, 107–113. [CrossRef]
4. World Health Organisation. Cancer—Key Facts. 2018. Available online: <https://www.who.int/news-room/fact-sheets/detail/cancer> (accessed on 1 March 2023).
5. Chabner, B.A.; Roberts, T.G., Jr. Timeline: Chemotherapy and the war on cancer. *Nat. Rev. Cancer* **2005**, *5*, 65–72. [CrossRef]
6. Krauss, G.; Schönbrunner, N.; Cooper, J. *Biochemistry of Signal Transduction and Regulation*; Wiley Online Library: Weinheim, NJ, USA, 2003; Volume 3.
7. Nguyen, K.-S.H.; Kobayashi, S.; Costa, D.B. Acquired Resistance to Epidermal Growth Factor Receptor Tyrosine Kinase Inhibitors in Non-Small-Cell Lung Cancers Dependent on the Epidermal Growth Factor Receptor Pathway. *Clin. Lung Cancer* **2009**, *10*, 281–289. [CrossRef]

8. Waldmann, T.; Schneider, R. Targeting histone modifications—Epigenetics in cancer. *Curr. Opin. Cell Biol.* **2013**, *25*, 184–189. [[CrossRef](#)]
9. Yang, X.-J.; Seto, E. Lysine Acetylation: Codified Crosstalk with Other Posttranslational Modifications. *Mol. Cell* **2008**, *31*, 449–461. [[CrossRef](#)]
10. Yang, X.J.; Grégoire, S. Metabolism, cytoskeleton and cellular signalling in the grip of protein N^ε- and O-acetylation. *EMBO Rep.* **2007**, *8*, 556–562. [[CrossRef](#)]
11. Sun, X.-J.; Man, N.; Tan, Y.; Nimer, S.D.; Wang, L. The Role of Histone Acetyltransferases in Normal and Malignant Hematopoiesis. *Front. Oncol.* **2015**, *5*, 108. [[CrossRef](#)]
12. Glauben, R.; Sonnenberg, E.; Zeitz, M.; Siegmund, B. HDAC inhibitors in models of inflammation-related tumorigenesis. *Cancer Lett.* **2009**, *280*, 154–159. [[CrossRef](#)]
13. Hanessian, S.; Auzzas, L.; Giannini, G.; Marzi, M.; Cabri, W.; Barbarino, M.; Vesci, L.; Pisano, C. ω -Alkoxy analogues of SAHA (vorinostat) as inhibitors of HDAC: A study of chain-length and stereochemical dependence. *Bioorganic Med. Chem. Lett.* **2007**, *17*, 6261–6265. [[CrossRef](#)]
14. Zhu, Y.; Li, H.-F.; Lu, S.; Zheng, Y.-X.; Wu, Z.; Tang, W.-F.; Zhou, X.; Lu, T. Investigation on the isoform selectivity of histone deacetylase inhibitors using chemical feature based pharmacophore and docking approaches. *Eur. J. Med. Chem.* **2010**, *45*, 1777–1791. [[CrossRef](#)]
15. Marks, P.A.; Rifkind, R.A.; Richon, V.M.; Breslow, R.; Miller, T.; Kelly, W.K. Histone deacetylases and cancer: Causes and therapies. *Nat. Rev. Cancer* **2001**, *1*, 194–202. [[CrossRef](#)]
16. Ekou, L.; Ekou, T.; Opalinski, I.; Gesson, J.P. Histone Deacetylase Inhibitors: Synthesis of Tetrapeptide Analogue SAHA/TPX. *E J. Chem.* **2011**, *8*, S79–S84. [[CrossRef](#)]
17. Grozinger, C.M.; Schreiber, S.L. Deacetylase Enzymes: Biological Functions and the Use of Small-Molecule Inhibitors. *Chem. Biol.* **2002**, *9*, 3–16. [[CrossRef](#)]
18. Miller, T.A.; Witter, D.J.; Belvedere, S. Histone deacetylase inhibitors. *J. Med. Chem.* **2003**, *46*, 5097–5116. [[CrossRef](#)]
19. Yoshida, M.; Horinouchi, S.; Beppu, T. Trichostatin A and trapoxin: Novel chemical probes for the role of histone acetylation in chromatin structure and function. *Bioessays* **1995**, *17*, 423–430. [[CrossRef](#)]
20. Methot, J.L.; Chakravarty, P.K.; Chenard, M.; Close, J.; Cruz, J.C.; Dahlberg, W.K.; Fleming, J.; Hamblett, C.L.; Hamill, J.E.; Harrington, P. Exploration of the internal cavity of histone deacetylase (HDAC) with selective HDAC1/HDAC2 inhibitors (SHI-1: 2). *Bioorganic Med. Chem. Lett.* **2008**, *18*, 973–978. [[CrossRef](#)]
21. Schäfer, S.; Saunders, L.; Eliseeva, E.; Velen, A.; Jung, M.; Schwienhorst, A.; Strasser, A.; Dickmanns, A.; Ficner, R.; Schlimme, S.; et al. Phenylalanine-containing hydroxamic acids as selective inhibitors of class IIb histone deacetylases (HDACs). *Bioorganic Med. Chem.* **2008**, *16*, 2011–2033. [[CrossRef](#)]
22. Islam, N.M.; Kato, T.; Nishino, N.; Kim, H.-J.; Ito, A.; Yoshida, M. Bicyclic peptides as potent inhibitors of histone deacetylases: Optimization of alkyl loop length. *Bioorganic Med. Chem. Lett.* **2010**, *20*, 997–999. [[CrossRef](#)]
23. Meinke, P.; Liberator, P. Histone Deacetylase: A Target for Antiproliferative and Antiprotozoal Agents. *Curr. Med. Chem.* **2001**, *8*, 211–235. [[CrossRef](#)]
24. Yoshida, M.; Matsuyama, A.; Komatsu, Y.; Nishino, N. From discovery to the coming generation of histone deacetylase inhibitors. *Curr. Med. Chem.* **2003**, *10*, 2351–2358. [[CrossRef](#)] [[PubMed](#)]
25. Bertrand, P. Inside HDAC with HDAC inhibitors. *Eur. J. Med. Chem.* **2010**, *45*, 2095–2116. [[CrossRef](#)]
26. Awad, S.M.; Zohny, Y.M.; Ali, S.A.; Mahgoub, S.; Said, A.M. Design, Synthesis, Molecular Modeling, and Biological Evaluation of Novel Thiouracil Derivatives as Potential Antithyroid Agents. *Molecules* **2018**, *23*, 2913. [[CrossRef](#)]
27. El-Naggar, A.M.; Abou-El-Regal, M.M.; El-Metwally, S.A.; Sherbiny, F.F.; Eissa, I.H. Synthesis, characterization and molecular docking studies of thiouracil derivatives as potent thymidylate synthase inhibitors and potential anticancer agents. *Mol. Divers.* **2017**, *21*, 967–983. [[CrossRef](#)]
28. Li, Y.; Wang, Y.; Xie, N.; Xu, M.; Qian, P.; Zhao, Y.; Li, S. Design, synthesis and antiproliferative activities of novel benzamides derivatives as HDAC inhibitors. *Eur. J. Med. Chem.* **2015**, *100*, 270–276. [[CrossRef](#)]
29. El-Kalyoubi, S.A.; Taher, E.S.; Ibrahim, T.S.; El-Behairy, M.F.; Al-Mahmoudy, A.M.M. Uracil as a Zn-Binding Bioisostere of the Allergic Benzenesulfonamide in the Design of Quinoline–Uracil Hybrids as Anticancer Carbonic Anhydrase Inhibitors. *Pharmaceuticals* **2022**, *15*, 494. [[CrossRef](#)]
30. El-Kalyoubi, S.; Agili, F.; Adel, I.; Tantawy, M.A. Novel uracil derivatives depicted potential anticancer agents: In Vitro, molecular docking, and ADME study. *Arab. J. Chem.* **2022**, *15*, 103669. [[CrossRef](#)]
31. El-Kalyoubi, S.A.; Ragab, A.; Abu Ali, O.A.; Ammar, Y.A.; Seadawy, M.G.; Ahmed, A.; Fayed, E.A. One-pot synthesis and molecular modeling studies of new bioactive spiro-oxindoles based on uracil derivatives as SARS-CoV-2 inhibitors targeting rna polymerase and spike glycoprotein. *Pharmaceuticals* **2022**, *15*, 376. [[CrossRef](#)]
32. El-Kalyoubi, S.; Agili, F.; Zordok, W.A.; El-Sayed, A.S.A. Synthesis, In Silico Prediction and In Vitro Evaluation of Antimicrobial Activity, DFT Calculation and Theoretical Investigation of Novel Xanthines and Uracil Containing Imidazolone Derivatives. *Int. J. Mol. Sci.* **2021**, *22*, 10979. [[CrossRef](#)]
33. El-Kalyoubi, S.; Agili, F. Synthesis, In Silico Prediction and In Vitro Evaluation of Antitumor Activities of Novel Pyrido [2, 3-d] pyrimidine, Xanthine and Lumazine Derivatives. *Molecules* **2020**, *25*, 5205. [[CrossRef](#)]

34. El-Kalyoubi, S.; Agili, F.; Youssif, S. Novel 2-Thioxanthine and Dipyrimidopyridine Derivatives: Synthesis and Antimicrobial Activity. *Molecules* **2015**, *20*, 19263–19276. [[CrossRef](#)]
35. Han, H.; Li, C.; Li, M.; Yang, L.; Zhao, S.; Wang, Z.; Liu, H.; Liu, D. Design, Synthesis, and Biological Evaluation of 8-Mercapto-3,7-Dihydro-1H-Purine-2,6-Diones as Potent Inhibitors of SIRT1, SIRT2, SIRT3, and SIRT5. *Molecules* **2020**, *25*, 2755. [[CrossRef](#)]
36. Mosmann, T. Rapid colorimetric assay for cellular growth and survival: Application to proliferation and cytotoxicity assays. *J. Immunol. Methods* **1983**, *65*, 55–63. [[CrossRef](#)]
37. Bandyopadhyay, D.; Okan, N.A.; Bales, E.; Nascimento, L.; Cole, P.A.; Medrano, E.E. Down-regulation of p300/CBP histone acetyltransferase activates a senescence checkpoint in human melanocytes. *Cancer Res.* **2002**, *62*, 6231–6239.
38. Bandyopadhyay, D.; Mishra, A.; Medrano, E.E. Overexpression of Histone Deacetylase 1 Confers Resistance to Sodium Butyrate-Mediated Apoptosis in Melanoma Cells through a p53-Mediated Pathway. *Cancer Res.* **2004**, *64*, 7706–7710. [[CrossRef](#)]
39. Wang, Z.; Qin, G.; Zhao, T.C. HDAC4: Mechanism of regulation and biological functions. *Epigenomics* **2014**, *6*, 139–150. [[CrossRef](#)] [[PubMed](#)]
40. Mai, A.; Perrone, A.; Nebbioso, A.; Rotili, D.; Valente, S.; Tardugno, M.; Massa, S.; De Bellis, F.; Altucci, L. Novel uracil-based 2-aminoanilide and 2-aminoanilide-like derivatives: Histone deacetylase inhibition and in-cell activities. *Bioorganic Med. Chem. Lett.* **2008**, *18*, 2530–2535. [[CrossRef](#)] [[PubMed](#)]
41. Wu, Y.; Wang, D.; Wang, X.; Wang, Y.; Ren, F.; Chang, D.; Chang, Z.; Jia, B. Caspase 3 is Activated through Caspase 8 instead of Caspase 9 during H₂O₂-induced Apoptosis in HeLa Cells. *Cell. Physiol. Biochem.* **2011**, *27*, 539–546. [[CrossRef](#)]
42. Denizot, F.; Lang, R. Rapid colorimetric assay for cell growth and survival: Modifications to the tetrazolium dye procedure giving improved sensitivity and reliability. *J. Immunol. Methods* **1986**, *89*, 271–277. [[CrossRef](#)]
43. Thabrew, M.I.; Hughes, R.D.; Mcfarlane, I.G. Screening of Hepatoprotective Plant Components using a HepG2 Cell Cytotoxicity Assay. *J. Pharm. Pharmacol.* **1997**, *49*, 1132–1135. [[CrossRef](#)]
44. Al-Rashood, S.T.; Hamed, A.R.; Hassan, G.S.; Alkahtani, H.M.; Almehezia, A.A.; Alharbi, A.; Al-Sanea, M.M.; Eldehna, W.M. Antitumor properties of certain spirooxindoles towards hepatocellular carcinoma endowed with antioxidant activity. *J. Enzym. Inhib. Med. Chem.* **2020**, *35*, 831–839. [[CrossRef](#)] [[PubMed](#)]
45. Kumar, P.; Nagarajan, A.; Uchil, P.D. Analysis of Cell Viability by the MTT Assay. *Cold Spring Harb. Protoc.* **2018**, *2018*, pdb-prot095505. [[CrossRef](#)]
46. Fournel, M.; Bonfils, C.; Hou, Y.; Yan, P.T.; Trachy-Bourget, M.-C.; Kalita, A.; Liu, J.; Lu, A.-H.; Zhou, N.Z.; Robert, M.-F. MGCD0103, a novel isotype-selective histone deacetylase inhibitor, has broad spectrum antitumor activity in vitro and in vivo. *Mol. Cancer Ther.* **2008**, *7*, 759–768. [[CrossRef](#)] [[PubMed](#)]
47. Heltweg, B.; Trapp, J.; Jung, M. In vitro assays for the determination of histone deacetylase activity. *Methods* **2005**, *36*, 332–337. [[CrossRef](#)]
48. Eldehna, W.M.; Hassan, G.S.; Al-Rashood, S.T.; Al-Warhi, T.; Altyar, A.E.; Alkahtani, H.M.; Almehezia, A.A.; Abdel-Aziz, H.A. Synthesis and in vitro anticancer activity of certain novel 1-(2-methyl-6-arylpyridin-3-yl)-3-phenylureas as apoptosis-inducing agents. *J. Enzym. Inhib. Med. Chem.* **2019**, *34*, 322–332. [[CrossRef](#)]
49. Yousef, R.G.; Sakr, H.M.; Eissa, I.H.; Mehany, A.B.; Metwaly, A.M.; Elhendawy, M.A.; Radwan, M.M.; ElSohly, M.A.; Abulkhair, H.S.; El-Adl, K. New quinoxaline-2 (1 H)-ones as potential VEGFR-2 inhibitors: Design, synthesis, molecular docking, ADMET profile and anti-proliferative evaluations. *New J. Chem.* **2021**, *45*, 16949–16964. [[CrossRef](#)]
50. Pozarowski, P.; Darzynkiewicz, Z. Analysis of Cell Cycle by Flow Cytometry. In *Checkpoint Controls and Cancer: Volume 2: Activation and Regulation Protocols*; Springer: Berlin, Germany, 2004; pp. 301–311.
51. Lo, K.K.-W.; Lee, T.K.-M.; Lau, J.S.-Y.; Poon, W.-L.; Cheng, S.-H. Luminescent Biological Probes Derived from Ruthenium(II) Estradiol Polypyridine Complexes. *Inorg. Chem.* **2007**, *47*, 200–208. [[CrossRef](#)]
52. Elkady, H.; Elwan, A.; El-Mahdy, H.A.; Doghish, A.S.; Ismail, A.; Taghour, M.S.; Elkaeed, E.B.; Eissa, I.H.; Dahab, M.A.; Mahdy, H.A.; et al. New benzoxazole derivatives as potential VEGFR-2 inhibitors and apoptosis inducers: Design, synthesis, anti-proliferative evaluation, flowcytometric analysis, and in silico studies. *J. Enzym. Inhib. Med. Chem.* **2022**, *37*, 403–416. [[CrossRef](#)]
53. Eray, M.; Mättö, M.; Kaartinen, M.; Andersson, L.C.; Pelkonen, J. Flow cytometric analysis of apoptotic subpopulations with a combination of Annexin V-FITC, propidium iodide, and SYTO 17. *Cytom. J. Int. Soc. Anal. Cytol.* **2001**, *43*, 134–142. [[CrossRef](#)]
54. Balah, A.; Ezzat, O.; Akool, E.-S. Vitamin E inhibits cyclosporin A-induced CTGF and TIMP-1 expression by repressing ROS-mediated activation of TGF- β /Smad signaling pathway in rat liver. *Int. Immunopharmacol.* **2018**, *65*, 493–502. [[CrossRef](#)]
55. Aborehab, N.M.; Elnagar, M.R.; Waly, N.E. Gallic acid potentiates the apoptotic effect of paclitaxel and carboplatin via over-expression of Bax and P53 on the MCF-7 human breast cancer cell line. *J. Biochem. Mol. Toxicol.* **2020**, *35*, e22638. [[CrossRef](#)] [[PubMed](#)]
56. Elnagar, M.R.; Walls, A.B.; Helal, G.K.; Hamada, F.M.; Thomsen, M.S.; Jensen, A.A. Functional characterization of α 7 nicotinic acetylcholine and NMDA receptor signaling in SH-SY5Y neuroblastoma cells in an ERK phosphorylation assay. *Eur. J. Pharmacol.* **2018**, *826*, 106–113. [[CrossRef](#)]
57. Guo, Y.; Tong, Y.; Zhu, H.; Xiao, Y.; Guo, H.; Shang, L.; Zheng, W.; Ma, S.; Liu, X.; Bai, Y. Quercetin suppresses pancreatic ductal adenocarcinoma progression via inhibition of SHH and TGF- β /Smad signaling pathways. *Cell Biol. Toxicol.* **2021**, *37*, 479–496. [[CrossRef](#)]

58. Jiao, C.; Chen, W.; Tan, X.; Liang, H.; Li, J.; Yun, H.; He, C.; Chen, J.; Ma, X.; Xie, Y.; et al. Ganoderma lucidum spore oil induces apoptosis of breast cancer cells in vitro and in vivo by activating caspase-3 and caspase-9. *J. Ethnopharmacol.* **2020**, *247*, 112256. [[CrossRef](#)]
59. Ma, C.; Taghour, M.S.; Belal, A.; Mehany, A.B.M.; Mostafa, N.; Nabeeh, A.; Eissa, I.H.; Al-Karmalawy, A.A. Design and Synthesis of New Quinoxaline Derivatives as Potential Histone Deacetylase Inhibitors Targeting Hepatocellular Carcinoma: In Silico, In Vitro, and SAR Studies. *Front. Chem.* **2021**, *9*, 725135. [[CrossRef](#)]
60. Elkady, M.A.; Doghish, A.S.; Elshafei, A.; Elshafey, M.M. MicroRNA-567 inhibits cell proliferation and induces cell apoptosis in A549 NSCLC cells by regulating cyclin-dependent kinase 8. *Saudi J. Biol. Sci.* **2021**, *28*, 2581–2590. [[CrossRef](#)]

Disclaimer/Publisher's Note: The statements, opinions and data contained in all publications are solely those of the individual author(s) and contributor(s) and not of MDPI and/or the editor(s). MDPI and/or the editor(s) disclaim responsibility for any injury to people or property resulting from any ideas, methods, instructions or products referred to in the content.